



THE UNIVERSITY *of* EDINBURGH

Edinburgh Research Explorer

In-situ resource utilisation manufacturing of optically transparent glass from lunar regolith simulant

Citation for published version:

Schleppi, J, Bromiley, G, Odling, N & Bennett, NS 2021, 'In-situ resource utilisation manufacturing of optically transparent glass from lunar regolith simulant', *Journal of Materials Science*.
<https://doi.org/10.1007/s10853-021-06059-x>

Digital Object Identifier (DOI):

[10.1007/s10853-021-06059-x](https://doi.org/10.1007/s10853-021-06059-x)

Link:

[Link to publication record in Edinburgh Research Explorer](#)

Document Version:

Peer reviewed version

Published In:

Journal of Materials Science

General rights

Copyright for the publications made accessible via the Edinburgh Research Explorer is retained by the author(s) and / or other copyright owners and it is a condition of accessing these publications that users recognise and abide by the legal requirements associated with these rights.

Take down policy

The University of Edinburgh has made every reasonable effort to ensure that Edinburgh Research Explorer content complies with UK legislation. If you believe that the public display of this file breaches copyright please contact openaccess@ed.ac.uk providing details, and we will remove access to the work immediately and investigate your claim.



In-Situ Resource Utilisation Manufacturing of Optically Transparent Glass from Lunar Regolith Simulant

Juergen Schleppi^{1, x}, Geoffrey Bromiley^y, Nic Odling^y, Nick S. Bennett^{1, z}

¹ Institute of Mechanical, Process and Energy Engineering, School of Engineering & Physical Science, Heriot Watt University, Edinburgh, EH14 4AS, United Kingdom

^x Maana Electric S.A., 5 Z.A.E Krakelshaff, L-3290, Bettembourg, Luxembourg

^y School of Geosciences, Edinburgh University, Grant Institute, King's Buildings, James Hutton Road, Edinburgh, EH9 3FE, United Kingdom

^z Centre for Advanced Manufacturing, Faculty of Engineering and Information Technology, University of Technology Sydney, Broadway, NSW 2007, Australia

Keywords: Lunar transparent glass, regolith simulant magnetic beneficiation, ISRU at lunar base, window glass made on the Moon, iron-bearing mineral removal, XRF and optical analysis

Abstract

International space agencies are aiming to establish permanent outposts on the lunar surface. For that purpose, new technologies and equipment are being developed which will enable and augment these mission goals. To increase the duration of a long-term planetary mission and to expand mission capabilities, the ability to manufacture transparent glass in-situ could be an important enabler on the lunar surface. Results presented in this work show that it is feasible to use different lunar regolith simulants to manufacture optically transparent glass by magnetically beneficiating regolith prior to processing. Beneficiated regolith simulant was melted, cast into glass nuggets which were then ground, lapped and polished into glass slides of 1mm thickness. The glass slides' surface roughness and geometry were measured, prior to optical analysis, which showed an average transmission of about 80 % of light in the wavelength range from 250 to 1250 nm. A comparable reference glass sample performed only about 9 % (absolute) better on average. From these results it seems viable to manufacture transparent glass from actual lunar regolith on the lunar surface as well, however, differences in regolith simulant and actual regolith still need to be fully explored – Regolith may be available on the lunar surface in unlimited quantities and therefore open up new strategic possibilities.

30 Introduction

31 Missions like the Lunar Orbital Platform – Gateway (LOP-G), seek to enable establishing a first
32 permanent human presence on the Moon and potentially Mars [1]. One of the goals for these missions
33 is to allow for the assembly and operation of surface missions by improving the “payload-to-lunar-
34 surface” metric and cost per kilogram compared to the Apollo missions.

35 During the Apollo missions the actual single launch payload-to-lunar-surface mass was about 6,000 kg
36 [2], which was the mass of the lunar lander after touch down (fuel of decent stage fully burnt). With
37 SpaceX’s new Starship, a fully reusable transport system, which shall be capable of servicing Earth’s
38 orbit as well as the Moon’s and Mars’s, this mass may now increase to 100+ metric tons when
39 refuelling in orbit around Earth [3]. Further, technology developed and tested for the international
40 space station (about 400 metric tons [4]) potentially enable smaller space station designs for a future
41 cis-lunar station in the range of about 50 metric tons [5]. Space-X’s Falcon 9 showed a 10-to-1
42 reduction in costs for development [6] and a 20-to-1 reduction in payload launch cost to Low Earth
43 Orbit (LEO) [7].

44 Despite these improvements, future human missions to the lunar surface will still be constrained by
45 mass transportation logistics [8] [9]. This is likely to be especially true if mining equipment has to be
46 flown [10] [11] to the lunar surface for, for example, mining water, aluminium, titanium, iron or oxygen
47 [12].

48 To allow for sustainable long-term space exploration and exploitation, means to lessen the mass
49 constraints have been devised. “In-Situ Resource Utilization” (ISRU) aims at utilising and harnessing
50 space resources for the purpose of creating items and products which enable space missions by
51 significantly reducing the mass, cost, and risk lunar surface exploration [13] [14]. Multiple concepts
52 and ideas for lunar missions using lunar resources [15] have been investigated up to the present day
53 [16], but only a small number of these studies focused on using local resources to manufacture
54 synthetic glass (fibres) [17] [18] [19] or even glass parts [20] [21] [22]. Utilising local lunar regolith to
55 manufacture transparent glass has only been investigated by considering pure anorthite, a lunar
56 regolith simulant, as an input material rather than bulk regolith simulant and actual regolith [23].

57 Artificially fabricated synthetic glass containers and glazing are amongst the oldest glass applications
58 on Earth. Ever since first using glass as building material for the first time a multitude of other
59 applications such as fibres, displays or electronic components have been developed. Glass can be
60 transparent, recycled, strong, chemically inert and is readily castable amongst other characteristics of
61 which most can be tailored to the specific needs today [24]. Making glass available as raw material on

62 the lunar surface may open possibilities for using glass in construction on the lunar surface. Possible
63 applications are windows, mirrors, solar cells, fibres or insulation foams, [23] which all require glass
64 material of different qualities and properties. For example, using synthetically manufactured glass as
65 backplate for front coated mirrors, glass composition is of minor importance compared to glass
66 surface quality. In comparison window glass or cover glass for, for example, solar cells, will require
67 optically transparent glass.

68 The goal of this work was to determine how transparent glass can be manufactured from bulk lunar
69 regolith by using artificial lunar regolith (regolith simulant) as starting material, and then to determine
70 the optical quality of the glass produced.

71 **Terrestrial basaltic glass, lunar glass and synthetic glass**

72 For this work, glasses found in nature (on the Moon and on Earth), are considered natural glasses and
73 glasses manufactured from sand, rocks and minerals are considered synthetic glass. Compared to
74 research conducted on terrestrial synthetic glasses, which are used in an increasing number of
75 applications on Earth, research conducted on natural (basaltic) glasses is comparably limited. On the
76 Moon glass has been found in quantities from 1-17 % in the mare regions and 5-25 % in the highland
77 regions [25]. There have been numerous geochemical studies of natural lunar glasses [26] [27],
78 principally aimed at determining how glasses and related volcanic products were formed, and what
79 they may indicate about the nature of the lunar interior [28] [29]. Studies on natural terrestrial glasses
80 also typically focus on geochemical characteristics, which can indicate conditions and geological
81 settings under which parental melts formed [30] [31] [32]. However, there has also been considerable
82 research on crystallisation behaviour of terrestrial basaltic glasses [33] [34] as well as their
83 physical/chemical [35] and magnetic [36] properties. Practical applications of synthetic basalt glass
84 are, for example, basalt fibre reinforced concrete [37] or immobilisation of transuranic wastes [38].
85 With respect to potential lunar applications, synthetic lunar glass can be produced from bulk lunar
86 material [19] and has already been used to manufacture synthetic glass substrate from artificial lunar
87 regolith (regolith simulant) for mirrors [20]. To the knowledge of the authors, only one study has been
88 conducted on manufacturing transparent synthetic lunar glass from anorthite [23] but not using a
89 regolith simulant as a starting point for manufacturing.

90 **Glass sheet manufacturing from regolith simulant**

91 The overall goal of this study was to manufacture a transparent glass sheet and to analyse its optical
92 properties, using available analogue lunar material. Previous work on basaltic glasses as a start did not
93 provide guidelines on the actual manufacturing process. Thus, terrestrial soda-lime glass

94 manufacturing was targeted, as this has been studied for centuries [39] [40]. Glass manufacturing on
95 Earth has changed much from early glass production [41], to the rise of the float glass process for
96 glazing [42], and many different types of glass have been developed and utilised. Other than the glass
97 composition and selected process, key parameters are processing temperature, material
98 combinations and correct cooling and annealing. This is in order to avoid, for example, bubble
99 formation or stress building up in the glass [43]. Due to the lack of practical experiments conducted
100 with basaltic glasses, it was required to develop a manufacturing process first before samples could
101 be produced and measurements could be conducted. The developed method will be described after
102 glass colour and the regolith beneficiation process have been discussed briefly.

103 **Basaltic glass colour**

104 Terrestrial basaltic glasses are typically black-brown-green and low transparency and lunar glasses are
105 variable in colour. Glass beads recovered during Apollo missions can be characterised based on Ti
106 content and colour, varying from green to orange-black [26]. Although multiple elements influence
107 glass colour, one of the elements having a major impact is iron [44] [45]. Typically, natural terrestrial
108 basaltic glasses have a green-brown/black taint which results primarily from the presence of Fe^{2+} and
109 Fe^{3+} . The presence of smaller amounts of other metal ions such as Cr, Mn, V, and Co may also
110 contribute to the colour. Only considering iron, synthetic glasses with very low, approx. 0.01 weight
111 percent (wt%) ferric oxide content do not show the blue-green coloration of typical window glass with
112 0.1 wt% ferric oxide content, especially for thicknesses $\gg 1\text{cm}$ [46]. Other applications require a
113 certain amount of iron oxide to manufacture highly coloured glasses such as car windows or beer
114 bottles with Fe_2O_3 contents of 1.4-4 wt% [47]. However, it should be noted that terrestrial glasses are
115 not typically synthesised from basaltic material, which is chemically complex and typically contains
116 appreciable amounts of iron. Other elements potentially impacting synthetic glass colour, even in
117 quantities as small as 0.1 wt%, are Ti, Cr and S [45] [44]. On Earth, a geologically complex environment
118 means that silica-rich, relatively Fe-poor material for making transparent glass is readily available. This
119 is not the case for the Moon, whose surface represents products formed by cooling on an extensive
120 magma ocean, overprinted by later, dominantly basaltic volcanism [26].

121 For this study, the prime focus was on removing iron oxide, and a secondary focus on removing
122 titanium, in order to synthesise transparent glass from lunar regolith simulant. The regolith simulants
123 used, which represent a range of six available regolith simulant materials (BP-1, EAC-1, FJS-1, JSC-1A,
124 JSC-2A, LHT-3M; more details in methods section), contained between 5.56 to 13.18 wt% Fe_2O_3 and
125 0.11 to 2.15 wt% TiO_2 in the raw bulk. Since these two were considered the prime contributor to the

126 colour of any glasses produced, the first step in trying to manufacture optically transparent glass from
127 these simulants was to remove as much Fe and Ti oxide from the input materials as possible.

128 **Beneficiation of regolith**

129 The goal of this work was to extract iron from a variety of six regolith simulants composed of igneous
130 rocks and minerals. Extraction of Fe, Si, Ti, H₂O, Al, Mg and O from extra-terrestrial sources has been
131 studied in the past and an overview is presented in [16]. Works reviewed in [16] include methods to
132 extract, for example, oxygen, water, and metals, and use principles such as vapor phase pyrolysis,
133 molten regolith electrolysis or carbothermal reduction. Some of these techniques are based on
134 terrestrial exploitation techniques, and although modifications to these conventional techniques may
135 work on the lunar surface, they are often energy intense and/or heavy on consumables and/or
136 complex. Further, the reviewed techniques in [16] sometimes considered pure minerals as inputs
137 rather than raw regolith, which seems unrealistic. However, it is more realistic to consider unaltered
138 regolith to be available as a resource. Unaltered regolith contains all minerals found at the landing site
139 which will probably show a range in both mineral and chemical composition. The yield of an extraction
140 method may suffer if it has to treat mineral fractions it was not designed for. However, only
141 considering certain minerals as input materials seems unrealistic in the authors' view as it is unlikely
142 that only a specific mineral, such as ilmenite, is found near the landing site in required purities and in
143 the right grain size spectrum.

144 Therefore, the authors suggest beneficiation of regolith material prior to extraction which will increase
145 the yield of the most often standalone solutions. Beneficiation is regarded as prior separation of a raw
146 material's minerals by means of mechanical processing, while using no consumables and as little
147 power as possible. Further, in searching for a suitable beneficiation process the goal was to find a low-
148 tech, reliable approach which would be capable of handling a wide variety of input materials.
149 Although, the mining industry has a wide range of potential beneficiation methods available, the
150 ultimate process was derived from a series of techniques geologist use to separate heavy, often Fe-
151 rich minerals from a sand/crushed or powdered sample.

152 **Geologists approach to separating high density minerals**

153 One approach to beneficiation is to process material to remove any denser minerals particularly
154 enriched in iron. Geologists often use three techniques to separate heavy minerals such as apatite
155 and/or zircon from a sand sample: shaker tables, electromagnetic separation, and heavy liquids. Since
156 a shaker table requires large amounts of water and comparably much space to work, it was deemed
157 unrealistic to be used on the lunar surface. Further, the impact of the reduced gravity environment on

158 this technique is not clear. Heavy liquids in general could work on the lunar surface and are an
 159 attractive approach as they use zero power, little space and are simple. However, each liquid can only
 160 separate a sample into two fractions, one fraction heavier and one lighter than the liquid. Thus, they
 161 are rather a crude method of modifying a concentrate composition. This led to using electromagnetic
 162 separation to split regolith (ore) into multiple different fractions with the goal to remove as much iron,
 163 as possible.

164 Materials and Methods

165 Preparing transparent glass samples from lunar regolith simulants required a multistep workflow as
 166 depicted in Figure 1. The following sections provide details with respect to every step on the work
 167 flow in Figure 1.

168 Selection of Simulants

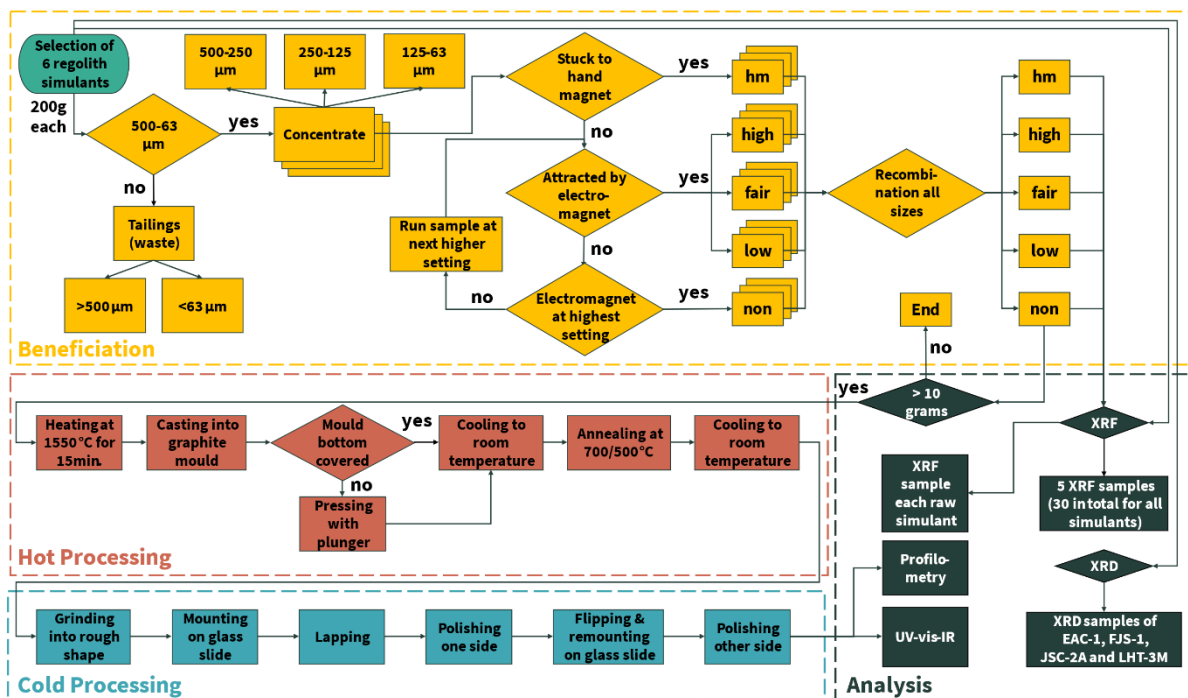
169 Six different lunar regolith simulants were selected with the aim to provide a variety of relevant
 170 compositions. This helped to test whether the developed process is sensitive to input material
 171 variations. The selected simulants were Black Point – 1 (BP-1), European Astronaut Centre – 1 (EAC-
 172 1), Fuji Japanese Simulant – 1 (FJS-1), Johnson Space Center - 1A (JSC-1A), Johnson Space Center - 2A
 173 JSC-2A, NASA/USGS - Lunar Highland Type - 3 Medium (LHT-3M). All but LHT-3M were mare simulants
 174 comprised primarily of igneous rock rich in iron oxide. LHT-3M is a highland simulant and is
 175 constructed from plutonic rock, rather than igneous rock. It was correspondingly iron sparse
 176 compared to the other five simulants. All simulants were designed to match Apollo sample grain size
 177 distribution but have been sourced from different suppliers and geolocations and are listed in Table
 178 1.

179 *Table 1 Overview of selected six regolith simulants*

Simulant	Description
BP-1	for Black Point – 1, was sourced from the Black Point basalt flow (San Francisco Volcanic Field) in northern Arizona. The sample was kindly provided by NASA Swamp Works (KSC) and is a mare simulant [48].
EAC-1	for European Astronaut Centre – 1, was sourced from the so called “Huehnerberg” quarry located in the Eifel region in Germany, south of Cologne. The sample was kindly provided by the European Astronaut Centre and is a mare simulant [49] [50].
FJS-1	for Fuji Japanese Simulant – 1, was procured from the Shimizu Corporation, which sourced it near Mount Fuji and is a mare simulant [51].
JSC-1A	for Johnson Space Center - 1A, was sourced from the volcanic ash field (San Francisco Volcanic Field) in northern Arizona. The sample was kindly provided by NASA Swamp Works (KSC) and is a mare simulant [52].
JSC-2A	for Johnson Space Center - 2A procured from Zybek Advanced Products in Westminster (CO) [53], USA and it was manufactured to be like JSC-1A and is a mare simulant.

LHT-3M	for NASA/USGS - Lunar Highland Type - 3 Medium, procured from and manufactured by Zybek Advanced Products in Westminster (CO) [53], USA, thus not directly linked to NASA or USGS any longer. The precursor simulants to NU-LHT-3M were the “medium 1 and 2”, NU-LHT-1/2M [54] which were manufactured and developed by USGS and NASA. All LHT family simulants are supposed to be roughly the same and all represent highland regolith simulants.
---------------	--

180 The oxide composition of each simulant, as provided by the manufacturer, is listed in Table 5 in
 181 supplemental material. For most simulants only a range for each oxide was provided by the
 182 manufacturer, rather than absolute values. Nevertheless, the manufacturer values provided enough
 183 information for the selection of the simulants. After arrival of the simulants, all raw materials have
 184 been sampled and XRF measurements were taken as well as XRD measurements on EAC-1, FJS-1, JSC-
 185 2A and LHT-3M. No XRD measurements have been taken on BP-1 and JSC-1A, however, JSC-1A is likely
 186 very similar to JSC-2A. Details on the measurement procedures are listed in the end of the methods
 187 section under analysis.



188
 189 *Figure 1 Workflow undergone by each of the selected six regolith simulants. After initial measurements, beneficiation via*
 190 *sieving and magnetic separation followed. Next, all beneficiated samples were analysed via means of XRF, prior to hot*
 191 *processing. Glass formed from the regolith simulants was cold processed to produce final glass slides which were then*
 192 *analysed by means of profilometry to determine roughness and flatness and in a UV-vis-spectrometer to determine reflectivity*
 193 *and transmission of the gasses.*

194 Beneficiation Method

195 200 grams of each regolith simulant sample have been dried, sieved and magnetically processed.
 196 After sieving three grain size groups for each selected simulant were available. Each of these grain
 197 size groups was processed separately via magnetic beneficiation.

198 **Drying and sieving**

199 Prior to magnetic separation, 200 grams (each) of all six simulants were dried at 220°C for two hours
200 and sieved afterwards.

201 By sieving, the simulants were divided into 6 groups, according to grain sizes: > 1000 µm, 1000-500
202 µm, 500-250 µm, 250-125 µm, 125-63 µm and < 63 µm. Afterwards, the remainders from three grain
203 size groups were used: 500-250, 250-125 and 125-63 µm and the other groups were discarded as
204 waste. The combined weight of these three grain size groups was different for all six simulants and
205 within the range 130 to 95 grams (details in Table 6 in supplemental material). Next, the remaining
206 amount for these three grain size groups was processed via (electro)magnetic separation.

207 **Magnetic separation**

208 As shown in Figure 1 the sieved and dried samples were first processed with a hand magnet (left in
209 Figure 3) and then using the electromagnetic setup depicted in Figure 2. Before using this
210 electromagnetic setup, the standard hand magnet (hm) depicted on the left in Figure 3 was used to
211 remove highly magnetic material from the bulk (samples marked “hm”). A total of approximately 100
212 grams of each regolith simulants split in three grain size groups was processed. For each of these,
213 three different electromagnetic field intensities were used during separation. Ultimately this led to
214 five samples types (hm, high, fair, low, non) for each grain size group, each with a different magnetic
215 susceptibility. After each run, the entered regolith simulant group was split into a magnetic and non-

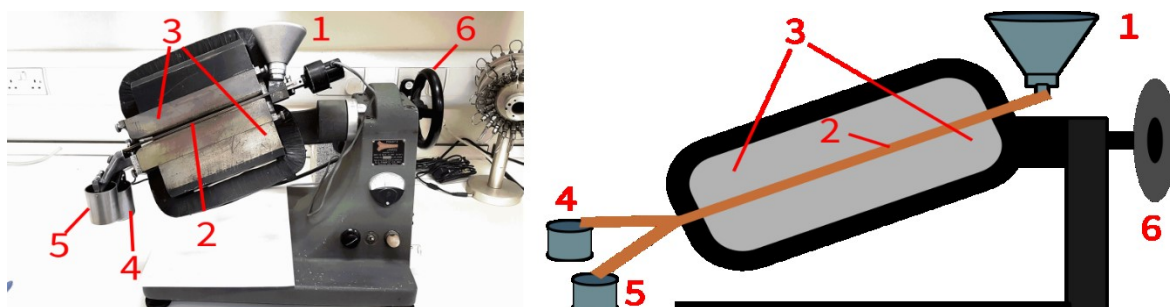
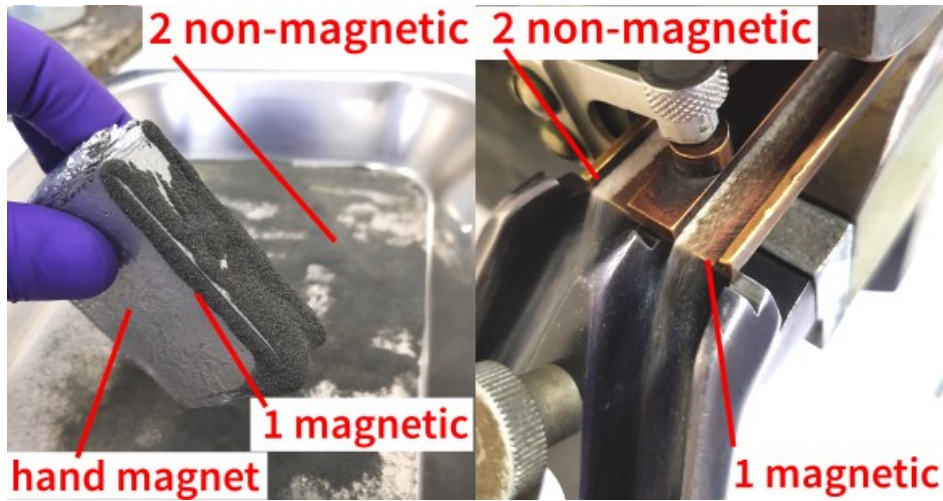


Figure 2 Electromagnetic separator, laboratory setup (left), schematically (right). Entry funnel (1) for regolith, copper slide (2), leading trough dedicated space in-between an electromagnet (3), at the end of the slide splitting regolith in two buckets containing non-magnetic (4) and magnetic material (5). Pitch and roll angle can be adjusted using the wheel (6).

216 magnetic fraction. In this case, “non-magnetic” simply refers to the fraction of material not
217 susceptible to exposure of the specific magnetic field used in that run. Hence, during another run,
218 processing regolith with a stronger magnetic field, parts of the regolith may be susceptible.

219 The three different grain size groups (500-250, 250-125 and 125-63 µm) were processed separately
220 for each simulant, to avoid contamination and clogging of the machine. This ultimately led to 6 regolith
221 simulants, each processed at 3 different grain sizes, and split into 5 categories of magnetic

222 susceptibility. Thus, $6*3*5 = 90$ samples were obtained. After processing, the 3 different grain sizes
223 for each simulant magnetic susceptibility subgroup were recombined, which led to $6*5 = 30$ samples.



224
225 *Figure 3 Two steps of magnetic separation, left separation utilising a hand magnet, right using an electromagnetic setup*
226 *both splitting the regolith into a magnetic (1) fraction and a non-magnetic fraction (2)*

227 The physical size of the electromagnet and slide led to a processing time of 4-5 hours for each grain
228 size group and led to the sample amounts listed in Table 6 in supplemental material. Each sample was
229 separated into five groups: hand magnet (HM), high, fair and low magnetic susceptibility and non-
230 magnetic (non) in the last run. Further, losses have been calculated based on the input amount of
231 sample.

232 During each separation step, samples were split into two groups, tailings and concentrate. Here,
233 tailings refer to the fraction of the sample which was magnetically susceptible during a processing
234 step. These tailings were removed and not further processed but an XRF measurement was taken. The
235 concentrate refers to the second group which was not magnetically susceptible during a processing
236 step. This group was processed further until the final step, which led to the “low” (tailings) and “non”
237 (concentrate) group. Hence, all measurements have been taken from the tailings but the last sample
238 “non” which was the concentrate. Note that prior to manufacturing a 1 g sample was taken from each
239 magnetically beneficiated group (30 in total) for XRF analysis.

240 [Hot Processing Method](#)

241 After the simulants had been separated into different groups, the “non” group was used to attempt
242 to manufacture a transparent glass sheet. Since LHT-3M-non was the only group which delivered
243 enough sample (>10 g) to manufacture a glass sheet of typical size, it was the only one leading to 3
244 “good” samples. However, despite the lack of a large amount of “non” sample, manufacture of
245 transparent glass from BP-1-non, FJS-1-non and JSC-2A-non was also attempted, as described below.

246 **Heating and casting**

247 Figure 4 shows parts of the heating and casting process for manufacturing a glass sheet from
248 magnetically beneficiated regolith simulants. On the left side in Figure 4 LHT-3M-non (1) and JSC-2A-
249 non (4) samples are depicted prior to processing and combining of gran size distributions. In the top
250 middle of Figure 4 a platinum crucible is shown next to a vial of LHT-3M-non prior to heating. Each
251 sample was processed following the same procedure. Samples of all grain sizes processed via magnetic
252 beneficiation were combined, placed in a platinum crucible, and heated at 1550 °C for 15 minutes in
253 a resistive heated furnace (temperature empirically determined as best working point temperature).
254 Then the crucible was removed from the furnace and the molten regolith sample was cast from the
255 platinum crucible into a graphite mould. Typically, the sample was then allowed to cool to room
256 temperature before being removed from the mould and further processed. Due to the small amount
257 of sample available for this experiment, two more samples of LHT-3M glass were manufactured by
258 entering a smaller amount of molten regolith into the graphite mould and pressing down on the
259 sample with a graphite plunger. These two resulting samples are shown in (3) and (6) in Figure 4 and
260 appear transparent. Also shown in subfigure 5 is a platinum crucible from the experiments with JSC-
261 2A with the small amount of JSC-2A-non, which also turned into a transparent glass.

262 No simulant other than LHT-3M, delivered an amount of more than 10 g of non-magnetic material.
263 However, BP-1, FJS-1 and JSC-2A delivered enough to attempt limited glass manufacturing as well.
264 Unfortunately, the thermal mass of these three samples was not sufficient to allow casting from a
265 platinum crucible, since the sample solidified in the crucible before it could be cast. Use of higher
266 temperatures (1700 °C) did not overcome this issue. Thus, samples were put into a graphite crucible
267 (known not to bond with regolith materials) and entered in the furnace at 1550 °C for only 3 minutes.
268 After removing the crucible from the furnace, the sample was kept in the crucible and a graphite
269 plunger was used to press down on the hot liquid glass to obtain a thin, elongated piece of glass similar
270 to (6) in Figure 4.

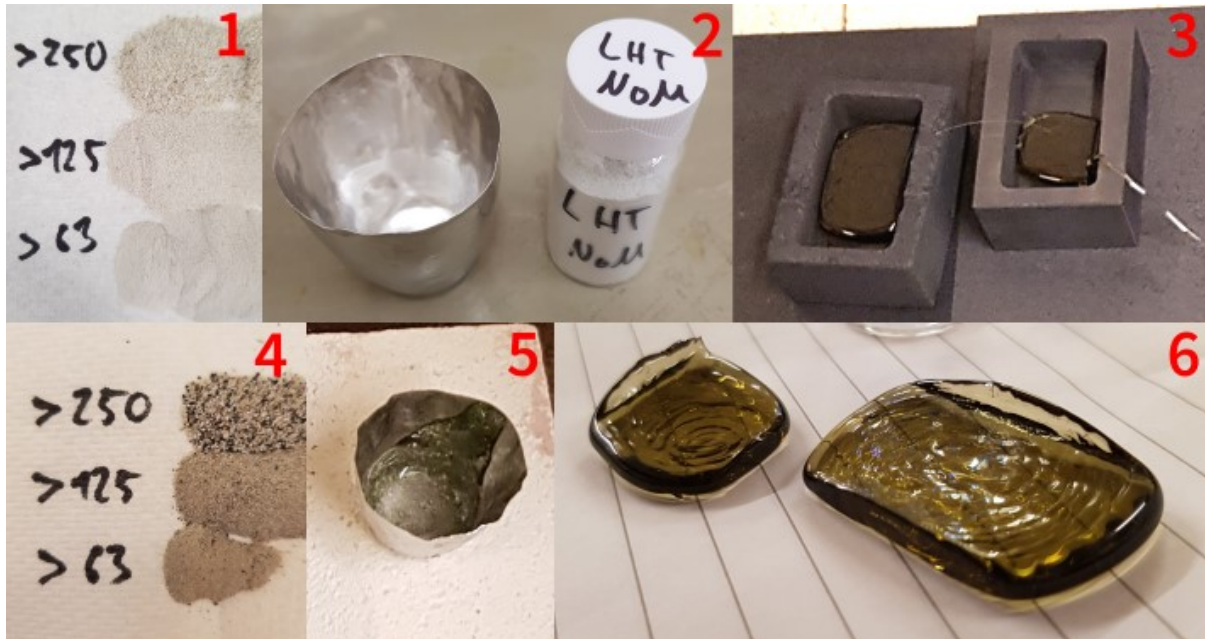


Figure 4 Iron sparse regolith “non” (after magnetic beneficiation) on the left (1 - LHT-3M and 4 - JSC-2A), iron sparse LHT-3M regolith next to crucible prior to melting next to platinum crucible (2), melted, cooled and compressed LHT-3M-non in the mould after processing (3) and after removing the samples from the crucible (6). Melted and cooled iron sparse JSC-2A in platinum crucible without contamination depicted in 5.

271 **Annealing**

272 After heating, melting, casting, and cooling to ambient temperature, a total of six samples (3 LHT-3M,
 273 1 BP-1, 1 FJS-1, and 1 JSC-1A) were obtained. For annealing these samples were all heated to 700 °C,
 274 starting at room temperature, at a rate of 170 °C/h. Next, samples were cooled from 700 to 550 °C at
 275 a rate of 150 °C/h until in a final step all samples were cooled back to room temperature at a rate of
 276 60 °C/h. Utilising this annealing process with samples of the given size or smaller avoided any breakage
 277 or cracking of the samples during processing or while handling them.

278 **Cold Processing Method**

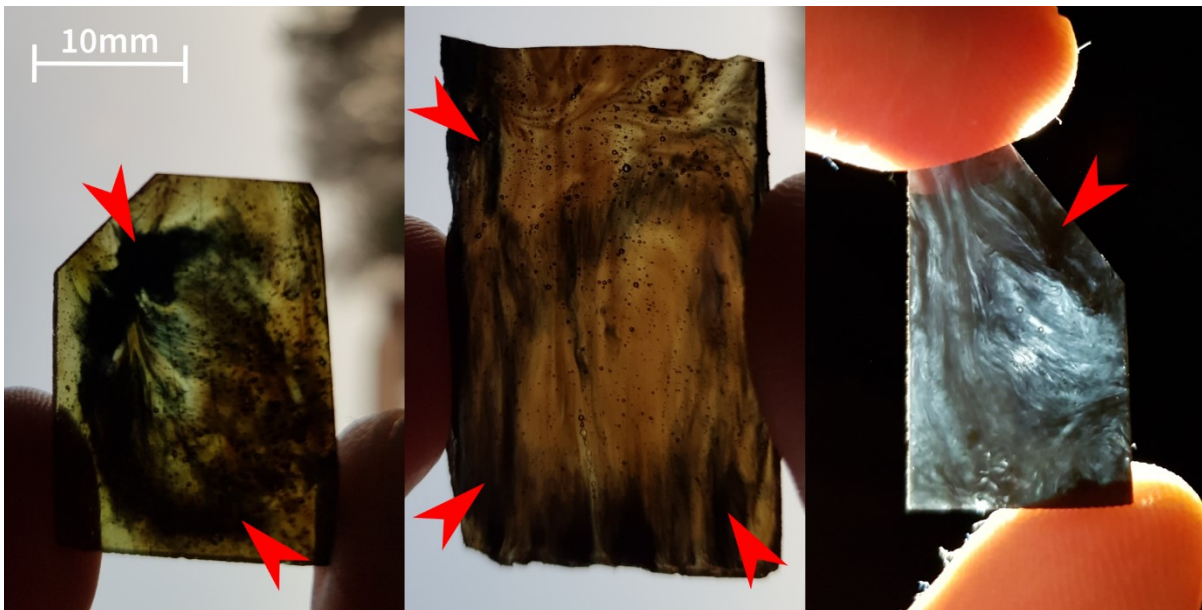
279 After heating and annealing, six shapeless samples were obtained. As shown in the workflow diagram
 280 in Figure 1 the next steps were cold processing the samples by means of grinding, lapping and
 281 polishing. Figure 5 shows the largest obtained raw sample (approx. 40*20*12mm) after casting (left)
 282 and after all cold processing steps (right). To achieve a flat, parallel glass slide it was necessary to grind
 283 the sample first with a 74 µm diamond disc into the rough shape of a glass slide. Next, the samples
 284 were mounted on a glass slide using Crystal-bond™. Then, the samples were processed on a lapping
 285 machine (to obtain parallel surfaces) with silicon carbide slurry to a thickness of 1.5 to 0.5 mm. In a
 286 last step samples were machine polished using 0.3 µm aluminium slurry. After polishing the first
 287 surface, each sample was heated, the Crystal-bond™ was removed, the sample separated from the
 288 glass slide, flipped and remounted on the sample holder. This ensured that both sides of the sample
 289 were as flat and smooth as possible, as required for optical measurements. All six (3 LHT-3M, 1 BP-1,

290 1 FJS-1, and 1 JSC-1A) samples could be processed into slides. However, latter three samples delivered
291 limited usable samples due to contamination shown in Figure 6 and discussed below.



292

293 *Figure 5 Transparent glass made from regolith simulant LHT-3M. Sample after casting and annealing (left) and after*
294 *processing (right).*



295

296 *Figure 6 Glass panes made of regolith simulants BP-1 (left), FJS-1 (middle) and JSC-2A (right). Partial transparency could be*
297 *achieved with visible black streaks of carbon (indicated by red arrowheads) which penetrated into the samples during*
298 *manufacturing from the graphite crucible.*

299 Analysis Methods

300 This section describes methods employed to measure mineralogical (XRD) and oxide (XRF) content of
301 the six regolith simulants utilised. Further, it describes methods used to measure the surface

302 properties (roughness and flatness) and the optical properties (reflectivity and transmission) of the
303 transparent glasses manufactured from some of these simulants.

304 **Mineralogic analysis of regolith samples via XRD and SEM**

305 X-ray powder diffraction (XRD) was used to identify phases in four unprocessed (EAC-1, FJS-1, JSC-2A
306 and LHT-3M) regolith simulant samples. All four samples were micro-ground and then spray dried
307 prior to being analysed on a Bruker D8 Advance diffractometer using Cu K-alpha radiation produced
308 by a 40kV accelerating voltage and a tube current of 40mA. The detector used was a sol-x energy
309 dispersive detector tuned for Cu K-alpha radiation, capable of quantitative and qualitative
310 identification of crystalline materials. Bruker Diffrac.EVA software in combination with latest
311 International Centre for Diffraction Data (ICDD) database was used for phase identification, and TOPAS
312 3.0 software for full profile Rietveld analysis and determination of phase proportions.

313 The proportion of glass/amorphous material present was not determined directly. Rather, its present
314 was first identified by visual identification in thin sections, then by its effect on peak intensities in the
315 XRD traces. The amount of amorphous material present in each sample was determined by a 'spiking'
316 method. For this, a known amount of an exotic mineral (in this case Calcite, CaCO_3) was added to the
317 sample. This composite sample was then scanned by XRD and the proportion of each mineral present
318 (including the CaCO_3 spike) determined by Rietveld analysis. As the spike mineral concentration is
319 known, the absolute amount of each mineral present can then be calculated by determining its
320 absolute concentration with respect to the known concentration of the spike mineral. Thus, when the
321 amounts of all the minerals present are summed, any deficit from 100% must either be accounted for
322 by a mineral phase not included in the Rietveld analysis or by the presence of a 'diluting' amorphous
323 phase. As all the diffraction peaks in the XRD traces have been assigned to mineral phases we discount
324 the possibility of a significant amount of an unknown phase(s) being present in the sample. Thus, any
325 deficit from 100% in the sum of the mineral assemblage must indicate the presence of an amorphous
326 phase.

327 In addition to the XRD measurements, thin sections of the samples were prepared for compositional
328 analyses using a scanning electron microscope with quantitative energy dispersive spectrometer
329 (SEM/EDX). In-situ compositional data was obtained using a Carl Zeiss SIGMA HD VP FEG SEM fitted
330 with Oxford AZtec EDX system.

331 **Analysis of regoliths' geochemical composition using XRF**

332 All six simulants used for this experiment were analysed using x-ray fluorescence spectroscopy (XRF)
333 to determine elemental composition. Two separate sets of measurements have been taken, one at

334 the beginning taken from each regolith simulant in its raw unaltered state and one after magnetic
335 beneficiation. Latter one led to a total of 30 samples as described earlier in the beneficiation methods.
336 This led to a total of 36 measurements.

337 Bulk composition of the sample was carried out by X-ray fluorescence using a Philips PW2404
338 wavelength dispersive sequential X-ray spectrometer at the School of GeoSciences at the University
339 of Edinburgh. The system is fitted with a rhodium anode end window X-ray tube operating at an
340 accelerating voltage of 50kV and a tube current of 50mA. Fused glass discs were prepared as described
341 in [55]. Samples were dried at 100°C and fused into glass discs using a borate flux (Johnson and Mathey
342 Spectroflux 105¹) in a ratio of 1:5, sample:flux.

343 For each of the 36 XRF measurements the loss on ignition (LOI) was determined, which is the weight
344 loss shown by a sample after heating, in air, to 1100°C for 20 minutes. This operation was carried out
345 immediately prior to fusion of the sample into glass discs as described above. LOIs are listed in Table
346 7 in supplemental material.

347 **Surface and parallelism analysis**

348 Surface roughness and flatness of two LHT-3M-non glass samples versus one 'off the shelf' microscopy
349 slide was determined using a profilometer. For this measurement a Taylor Hobson Talysurf-5 modular
350 system was utilised which records the results on electro-sensitive chart paper, which was then
351 digitised. The systems sensitivity tolerance is $\pm 2.0\%$ and is driven by a synchronous motor. The
352 instrument's stylus made one trace across the surface of about 1mm in the centre of the sample and
353 along the longest dimension of the sample.

354 The parallelism of all the samples (microscopy slide, 3 LHT-3M samples & BP-1, FJS-1 and JSC-2A
355 samples) was determined by measuring thickness of each sample at each corner using a micrometre
356 screw and calculating the difference in thickness between these points.

357 **UV-vis-IR spectroscopy**

358 Reflectivity and transmission of the six regolith glasses and one reference microscopy slide were
359 determined over a wavelength range of 350 -1250 nm by using a PerkinElmer Lambda 950 UV-vis-NIR
360 spectrometer.

¹ Spectroflux 105 consists of a mixture of 47 % Lithium tetraborate, Li₂B₄O₇, 37 % Lithium carbonate (Li₂O) and 16 % of La₂O₃, Lanthanum oxide as an X-ray heavy absorber.

361 **Results**

362 During the process of preparing a transparent glass slide from regolith simulant, three main
 363 measurements have been conducted. First, the analysis of the regolith samples composition prior and
 364 after the magnetic beneficiation. Second, the samples surface roughness after grinding, lapping and
 365 polishing. Third, the optical properties of each sample with a focus on transmission measurements.
 366 All percent values in this chapter are weight percent (wt %) if not indicated otherwise.

367 **XRD**

368 Results obtained from XRD analysis of four (EAC-1, FJS-1, JSC-2A and LHT-3M) of the initial, raw and
 369 unaltered regolith samples is shown in Table 2. Additionally, for reference supplier values for BP-1 are
 370 also included.

371 *Table 2 XRD results overview, values for mineral groups are displayed in wt %*

Group	BP1^M	EAC1	FJS1	JSC2A	LHT3
Plagioclase	57.7	13.8	55.9	45.7	66.6
K Feldspar	7.3	13.4	5.0	5.0	2.9
Pyroxene	13.8	35.5	26.3	6.8	24.4
Olivine	12.9	13.3	5.0	11.9	1.3
Oxide Minerals	8.3	2.0	1.5	0.6	0.3
Glass	na	14.4	0.7	23.9	0.0
Mica	na	3.3	3.2	1.8	0.9
Alteration	na	4.3	2.4	4.4	3.8
Sum	100.0	100.0	100.0	100.0	100.0

^M Manufacturer Data [56]

372 Mineral phases detected by XRD with Rietveld refinement include numerous members of solid
 373 solution series, and can be categorised into minerals groups, as listed in Table 3.

374 *Table 3 Detected minerals groups and individual minerals by XRD with Rietveld refinement*

Group	Minerals contained
Plagioclase	Albite, Andesine An50, Anorthite, Bytownite An85, Labradorite An65, Oligoclase An16
K Feldspar	Microcline maximum, Orthoclase, Sanidine Na0.07, Nepheline
Pyroxene	Aegirine, Augite, Diopside, Enstatite, Pigeonite
Olivine	Forsterite (iron)
Oxide Minerals	Ilmenite, Titanomagnetite
Glass	Amorphous material
Mica	Annite Mica, Muscovite 2M1
Alteration	Chlorite, Illite, Kaolinite (BISH), Phlogopite

375 XRF

376 The results of the XRF analysis of the initial 6 raw, unaltered regolith simulants, as well as the 30
 377 magnetically beneficiated samples are listed in Table 5. Again, the categories for the 30 magnetically
 378 altered samples are hm, low, fair, high and non, and for the raw unaltered regolith its unaltered name
 379 is used. The table shows the unaltered composition of each simulant in the first row (full simulant
 380 name) and the according changes for each level of magnetic treatment. Further, the according loss on
 381 ignition is listed with every sample.

382 *Table 4 XRF analysis results of magnetically altered regolith simulant samples, shown in wt%, not corrected for LOI.*
 383 *Unaltered samples are shown in the first line named after the simulant, results of the tailings of each step are shown as*
 384 *“hm”, “high”, “fair” and “low” as well as the final concentrate is shown under “non”.*

Sample	SiO₂	Al₂O₃	Fe₂O₃	MgO	CaO	Na₂O	K₂O	TiO₂	MnO	P₂O₅	LOI	Total
BP-1	46.13	15.91	11.96	6.31	10.28	3.08	1.01	2.04	0.17	0.39	2.04	99.32
B-hm	46.14	15.86	13.86	6.52	9.25	3.28	1.04	2.56	0.19	0.42	0.88	100.01
B-high	46.82	15.56	11.58	7.27	10.08	2.98	0.99	1.68	0.17	0.37	2.22	99.73
B-fair	46.44	14.74	9.98	8.29	11.11	2.71	0.93	1.22	0.15	0.31	3.76	99.63
B-low	45.85	15.20	5.03	3.96	15.93	2.47	0.95	0.76	0.09	0.23	9.11	99.56
B-non	45.78	19.29	1.39	1.12	19.08	2.50	0.44	0.18	0.03	0.06	9.80	99.66
EAC-1	43.58	11.45	12.66	14.08	10.18	2.62	1.18	2.15	0.21	0.59	1.40	100.11
E-hm	44.20	12.96	12.26	11.58	10.79	2.67	1.35	2.37	0.19	0.67	1.19	100.24
E-high	43.63	9.21	13.27	18.66	8.58	1.51	0.99	1.45	0.24	0.42	1.74	99.69
E-fair	41.93	2.53	13.99	36.40	3.08	0.03	0.27	0.28	0.24	0.08	1.08	99.90
E-low	46.80	5.53	7.45	23.75	8.44	0.67	0.96	0.38	0.19	0.11	6.05	100.34
E-non	40.78	5.82	1.44	5.27	23.39	0.84	1.37	0.13	0.14	0.08	20.31	99.57
FJS-1	49.82	16.56	12.90	5.91	9.71	2.42	0.66	1.46	0.20	0.28	-0.25	99.67
F-hm	49.40	14.50	14.85	6.73	9.15	2.15	0.76	1.75	0.22	0.32	-0.19	99.66
F-high	50.32	18.35	9.81	7.04	10.06	2.29	0.53	0.69	0.16	0.21	-0.16	99.31
F-fair	49.75	17.33	10.03	10.15	10.03	1.92	0.32	0.44	0.17	0.11	-0.37	99.88
F-low	51.09	25.25	4.42	3.40	12.25	2.85	0.28	0.24	0.07	0.06	-0.04	99.88
F-non	51.81	29.39	1.42	0.01	13.30	3.36	0.25	0.10	0.02	0.02	0.22	99.89
JSC1-A	46.76	16.24	12.62	8.57	9.90	2.91	0.82	1.80	0.19	0.70	-0.46	100.04
J1-hm	46.66	16.32	12.60	7.28	10.16	3.07	0.87	1.92	0.19	0.76	-0.46	99.39
J1-high	46.26	15.50	13.14	9.87	9.34	2.86	0.80	1.76	0.20	0.68	-0.57	99.83
J1-fair	46.36	15.58	12.71	10.22	9.44	2.81	0.76	1.67	0.19	0.64	-0.67	99.71

J1-low	47.89	21.05	8.67	4.76	11.88	3.20	0.64	1.31	0.13	0.50	-0.20	99.82
J1-non	39.53	21.46	1.29	1.03	22.87	1.94	0.16	0.18	0.02	0.19	11.11	99.77
JSC-2A	46.28	16.63	13.18	7.98	9.65	3.11	0.82	1.83	0.20	0.71	-0.79	99.59
J2-hm	46.32	15.94	13.62	8.15	9.59	3.05	0.88	1.96	0.20	0.77	-0.65	99.82
J2-high	45.75	15.13	13.54	10.29	8.94	3.35	0.84	1.76	0.20	0.68	-0.64	99.86
J2-fair	46.21	15.87	12.76	10.72	9.18	2.72	0.72	1.57	0.18	0.61	-0.70	99.82
J2-low	46.55	17.26	11.60	9.81	9.78	2.72	0.65	1.42	0.17	0.54	-0.46	100.05
J2-non	37.89	18.93	0.93	0.90	24.29	1.97	0.29	0.13	0.02	0.21	14.05	99.60
LHT-3M	49.34	21.59	5.56	9.49	12.54	1.04	0.08	0.11	0.09	0.02	0.12	99.97
L-hm	49.30	16.64	9.17	13.00	10.93	0.52	0.05	0.14	0.14	0.02	-0.36	99.56
L-high	50.27	12.38	8.36	17.33	8.24	0.34	0.03	0.14	0.15	0.00	2.22	99.47
L-fair	50.82	14.82	7.50	15.64	9.83	0.45	0.04	0.13	0.14	0.00	0.21	99.59
L-low	48.23	27.46	2.76	4.52	15.22	1.07	0.06	0.06	0.05	0.01	0.26	99.70
L-non	47.32	33.13	0.72	n.d.	17.22	1.32	0.07	0.03	0.01	0.01	0.25	100.06

n.d. = not detected

385 **Surface Properties**

386 Surface roughness of two LHT-3M samples were measured versus one 'off the shelf' microscopy
387 slide. Results are depicted in Figure 8 and show the three samples over the distance of up to 0.9 mm
388 and a deviation from the mean line within 15 to -20 nm. LHT-3M samples are depicted in green and
389 the microscopy slide in violet.

390 Thicknesses measurements obtained with a micrometre screw reach from 1.4 mm to about 0.8 mm
391 and differences between corners of regolith samples are 0.040 to 0.010 mm. Detailed values can be
392 found in Table 9 in the supplementary material.

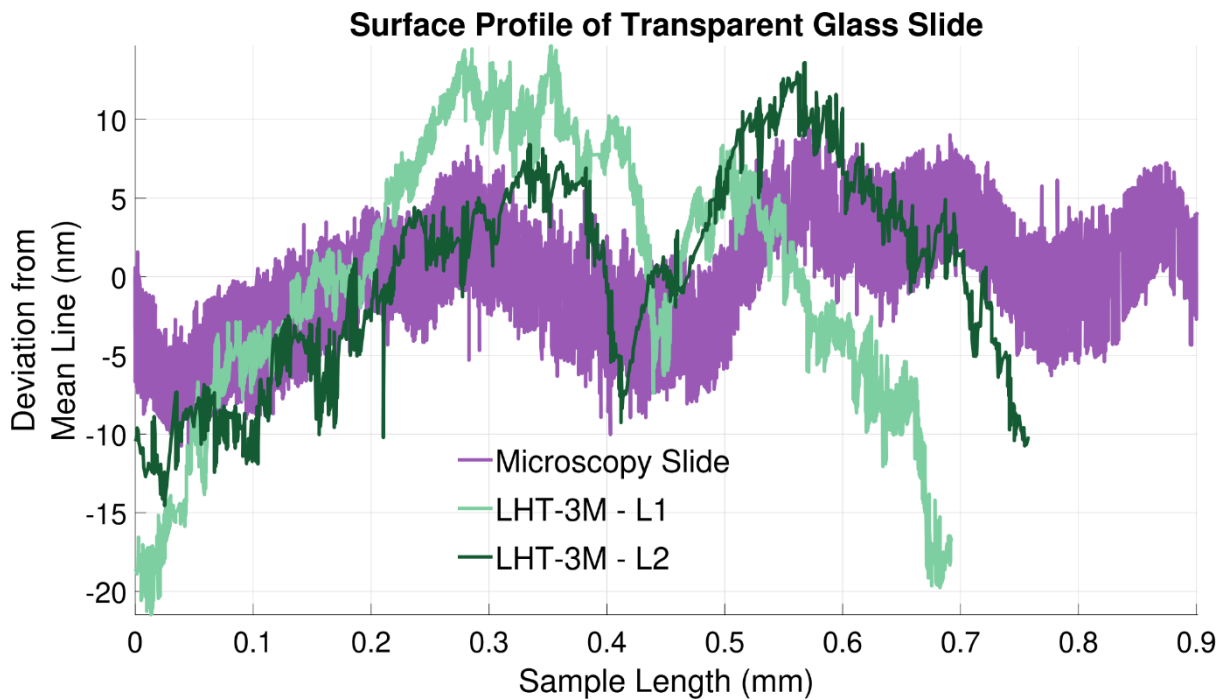


Figure 7 Surface roughness of two polished transparent substrate made from LHT-3M (shades of green) which has been magnetically treated to remove iron oxide. Reference; 'off the shelf' microscopy slide (violet). The abscissa shows length on the samples surface in mm and the ordinate deviation from the mean line in nm.

393 **UV-vis-IR results**

394 Results of reflectivity measurements are depicted in Figure 10 and results of the transmission in Figure
 395 9. Also included on Figure 9 is an AM0 spectrum, superimposed on the figure, showing the spectrum
 396 which would be seen by a solar cell or a sample in space, in the vicinity of Earth.

397 From the results in Figure 9 average transmissions over the entire wavelength range have been
 398 calculated and are listed in Table 8 in supplementary material.

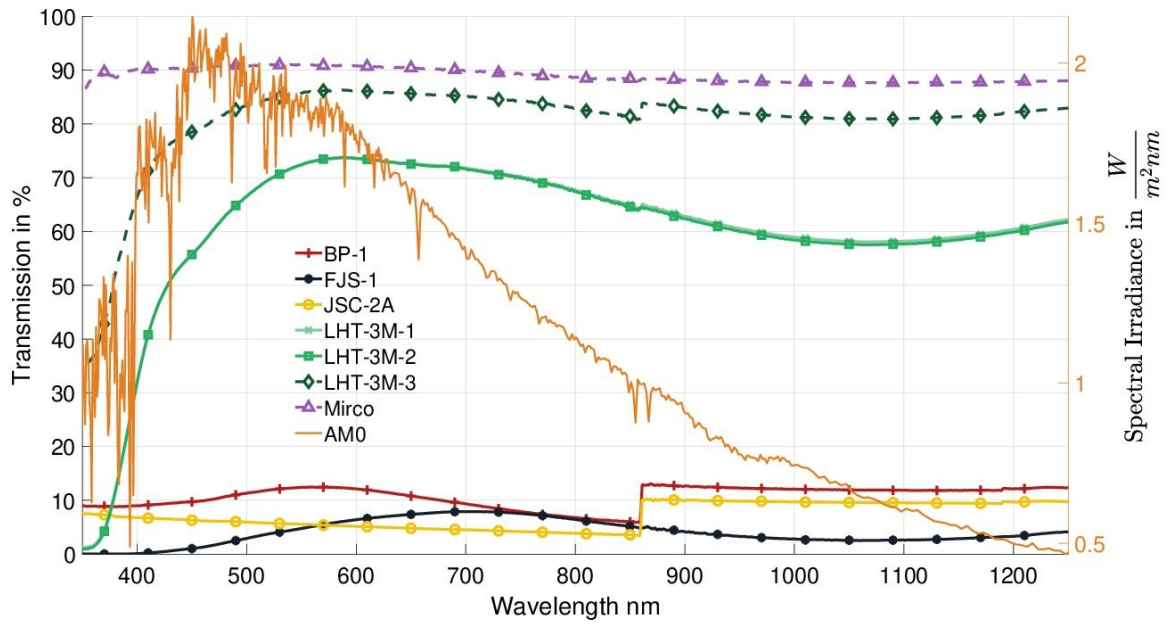
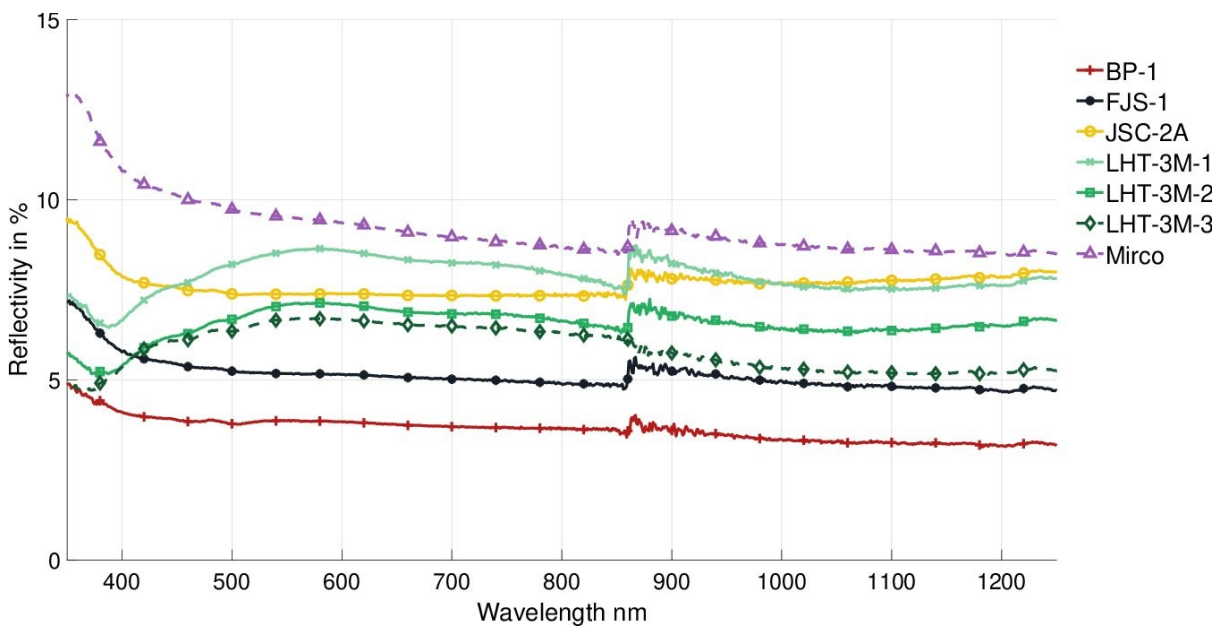


Figure 8 Transmission of transparent regolith simulant glass substrates over a wavelength range of 350 to 1250 nm, made from four different regolith simulants and compared to a microscopy slide ("Micro"), superimposed by the solar spectrum AM0 which would be seen by a solar cell or a sample in space, in the vicinity of Earth. Lines of samples LHT-3M-1 and LHT-3M-2 coincide.

399

Figure 9 Reflectivity of transparent regolith simulant glass samples over a wavelength range of 350 to 1250 nm, made from four different regolith simulants and compared to a microscopy slide ("Micro").



400

401 **Discussion**

402 **Beneficiation**

403 Drying and sieving went as expected with the only exception that the large amount of fine grained
 404 regolith (<63 μm) led to longer processing times in the sieving tower. This was to allow for all the fine

405 grain material to migrate to the bottom of the sieve tower and not be incorrectly incorporated in
406 another grain size group.

407 For magnetic separation, differences were observed between the different grain sizes processed. The
408 smallest grains sizes tended to clog the system more often than the larger ones, and different grain
409 sizes sometimes led to different yields. However, this latter observation requires confirmation from a
410 larger number of data points as well as repetitions for quantitative results. The overall yields for each
411 simulant and all grain sizes recombined (500-63 μm) are shown in Table 6 in supplemental material.
412 Due to cleaning and unblocking the system for some sample groups it was necessary to rerun these
413 groups up to three times. This added to the long processing times (4-5 hours each run) which were
414 inherent to the utilised system. Further, the long processing time and small amounts of about 100
415 grams of regolith which could only be processed in a reasonable time led to, in some cases, less than
416 1 gram of sample in a specific group. Also apparent from Table 6, all mare simulants have comparably
417 low yields in the non-magnetic ("non") area. It is further apparent that, the sample with the highest
418 yield in the non-magnetic group is the highland simulant LHT-3M. Looking at the manufacturer's data
419 in Table 5 (supplemental material) and the obtained XRF measurements in Table 4, LHT-3M also has
420 the lowest iron oxide content of all simulants. Although the yields in Table 6 may suggest that more
421 iron oxide sparse input material seems to produce more non-magnetic material, which can be used
422 for glass manufacturing, it is important to consider that these oxides are contained in minerals rather
423 than in individual oxide form. Hence, the mineral composition of an input material will be the driver
424 for how well a regolith (simulant) separates. With respect to manufacturing glass from iron free/iron
425 sparse material, the method used works but for most simulants processed, a starting amount of 100
426 grams was not enough to separate a sufficient quantity of material to manufacture a sheet of glass.
427 Typically, about 10 grams of processed material was enough to manufacture a glass sheet of 30*20*1
428 mm, and only LHT-3M provided this amount. This was after recombination of the three different grain
429 size groups back to 30 samples. This was also necessary to obtain enough material to be able to obtain
430 XRF data for all 30 samples.

431 Although, beneficiation was successful, as shown in the discussion of the XRF results later, it remains
432 to be tested whether the process would be feasible in a lunar environment with reduced gravity, which
433 will impact transport of the grains during processing, and at temperatures as low as $< -100\text{ }^{\circ}\text{C}$ [57] [58]
434 [59], where magnetic susceptibility of minerals may change [60] [61]. Further, it seems viable to
435 automate this process and to reduce power consumption by possibly utilising only permanent
436 magnets instead of electromagnets, both to increase mission capabilities further.

437 Hot processing

438 While melting and casting LHT-3M-non and JSC-2A-non it was noticed that JSC-2A-non had a slight
439 blue tint compared to the greenish taint of the LHT-3M-non sample. Glass colouration is complex, so
440 it is hard to tell what exactly causes a certain colouration without measuring the trace element
441 amounts as well. Unfortunately, such measurements require about 3-4 grams of sample which were
442 not available, and therefore, not conducted.

443 Annealing parameters were determined empirically, to work for all regolith simulants at the same
444 time. Since annealing temperature is related to the glass transition temperature of a regolith/glass,
445 energy saving potential exist for future experiments and applications. Via optimisation and tailoring
446 of the process temperature to the actual regolith glass transition temperature (e.g. 620 °C for JSC-2A
447 [62]) and composition this potential can be explored in the future. For this experiment run the process
448 efficiency was of secondary importance and sample quality had priority.

449 Carbon contamination

450 For manufacturing of the contaminated samples shown in Figure 6 the heating time was reduced to 3
451 minutes (compared to 15 for LHT-3M-non) since their mass was smaller (< 6 g) compared to the 40
452 grams of LHT-3M non-magnetic material. The further intention was to keep the reaction time between
453 graphite and the sample material to a minimum. However, despite these measures, the process
454 resulted in variable carbon contamination of the glasses. Carbon contamination is clearly visible in
455 Figure 6 as black streaks or lines and blocks most of the light from being transmitted. However,
456 transparent spots are visible in-between the graphite streaks. This suggests that it should be possible
457 to also manufacture transparent glass from other regolith compositions than LHT-3M, a highland
458 simulant. The fact that carbon contamination can still be seen after polishing of the samples suggests
459 that it is not simply surface contamination. Hence, carbon likely penetrated the glass entirely during
460 heating in the furnace. Presence of a free carbon phase likely means that the samples are fairly
461 reduced, as carbon will readily react with oxygen in the air to produce CO₂ and CO. Furthermore, this
462 also implies that graphite crucibles cannot readily be used for heating/processing samples at high
463 temperatures since the crucible will interact with the sample in the form of a carbothermal reduction.
464 An exception can be made for using graphite as moulds for casting, since temperature drops rapidly
465 during casting which does not allow for any reduction to take place.

466 Glass colour is different for all of these samples. This is likely a result of trace elements being contained
467 in the samples which give the glasses their green, brown, and blue colours. To be able to tell which
468 elements are responsible for the colouration, enough sample for a trace element analysis would need
469 to be collected. However, it is likely that green-brown colouration arises due to the presence of iron,

470 as commonly noted in terrestrial basaltic glasses. Green colouration due to the presence of Ti^{3+} is,
471 however, noted in reduced clinopyroxene from the Allende meteorite [63] . A blue colouration may
472 be due to the presence of Ti, especially in its reduced form Ti^{3+} . Blue colouration due to Ti-Ti
473 intervalence charge transfer, or due to Ti^{3+} colour centres, is commonly noted in other material [64].

474 Cold processing

475 Although cold processing led to suitable glass samples for analysis, it is noted that the described cold
476 processing process utilised a number of consumables not readily available on the Moon. Thus,
477 alternative hot manufacturing processes may be utilised in the future to obtain an ideal surface in one
478 shot. Terrestrially this can be observed in the float glass process for example. Alternatively, or
479 additionally locally available materials (regolith) may be used as grinding, lapping and polishing agent
480 instead of the described materials.

481 Analysis of effects of magnetic beneficiation

482 This section discusses the results of XRD/SEM, XRF, surface and optical analysis.

483 Discussion of magnetic beneficiation using XRF, XRD and SEM results

484 Prior to the discussion it was pointed out that the LOIs during XRF sample preparation, listed in Table
485 7 in supplemental material, show especially high (more than 10 % and in one case (EAC-1, non) in
486 excess of 20 %) losses for samples labelled with “-non”, the least magnetic samples. High LOI values
487 in a sample could be derived from water in the sample (either adsorbed or structural water in minerals
488 such as micas and amphiboles), or contaminants, such as polymers from packaging and/or bottling, as
489 well as contained organic materials. Water is however, not very likely since samples have been dried
490 prior to processing. The other materials are typically not magnetic and will collect in the non-magnetic
491 group and lead to the weight loss during sample preparation. Although, on the lunar surface organic
492 contamination of any kind are unknown so far, foreign materials entering the regolith concentrate
493 during processing, from the process itself may need to be accounted for when utilising magnetic
494 separation.

495 XRD and SEM data confirmed the occurrence of pyroxene, feldspar, olivine, alteration phases and
496 oxide minerals in all simulants and the likely occurrence of larger amounts (>10wt%) glass in EAC-1
497 and JSC-2A. Respectively, it is very likely that JSC-1A also contains a similar amount of glass and other
498 minerals since these two simulants are very similar by design. From this list of minerals, looking at the
499 oxide content obtained by means of XRF conclusion can be drawn from the oxide content changes
500 with respect to the changes in the minerals content of a regolith simulant.

501 Prior to discussing changes caused by the beneficiation process, the manufacturer values are
502 compared with respect to the obtained raw, unaltered regolith XRF measurement results.
503 Manufacturer values of simulants supposed oxide composition are provided in Table 5 in
504 supplemental material. In there, the simulant with the initially highest amount of iron oxide is FJS-1
505 (13.1 wt%) and the one with the lowest LHT-3M (4.2 wt%). However, the actual measurements of the
506 raw regolith, shown in the according first line for each simulant in Table 4, show that JSC-2A had the
507 highest iron oxide content with 13.18 wt% and FJS-1 only contained 12.9 wt%. Further, LHT-3M still
508 showed the lowest initial iron oxide content but with 5.56 wt% rather than 4.2 wt%. The example of
509 iron oxide content is only one where oxide values provided by the manufacturers differ significantly
510 from the actual values of the shipped material. Since standards and quality control are not yet
511 established in the field of regolith simulants, it will therefore always be necessary to determine the
512 geochemical composition of a newly shipped batch, prior to utilisation, to allow to draw conclusion
513 and to establish comparability between scientific works.

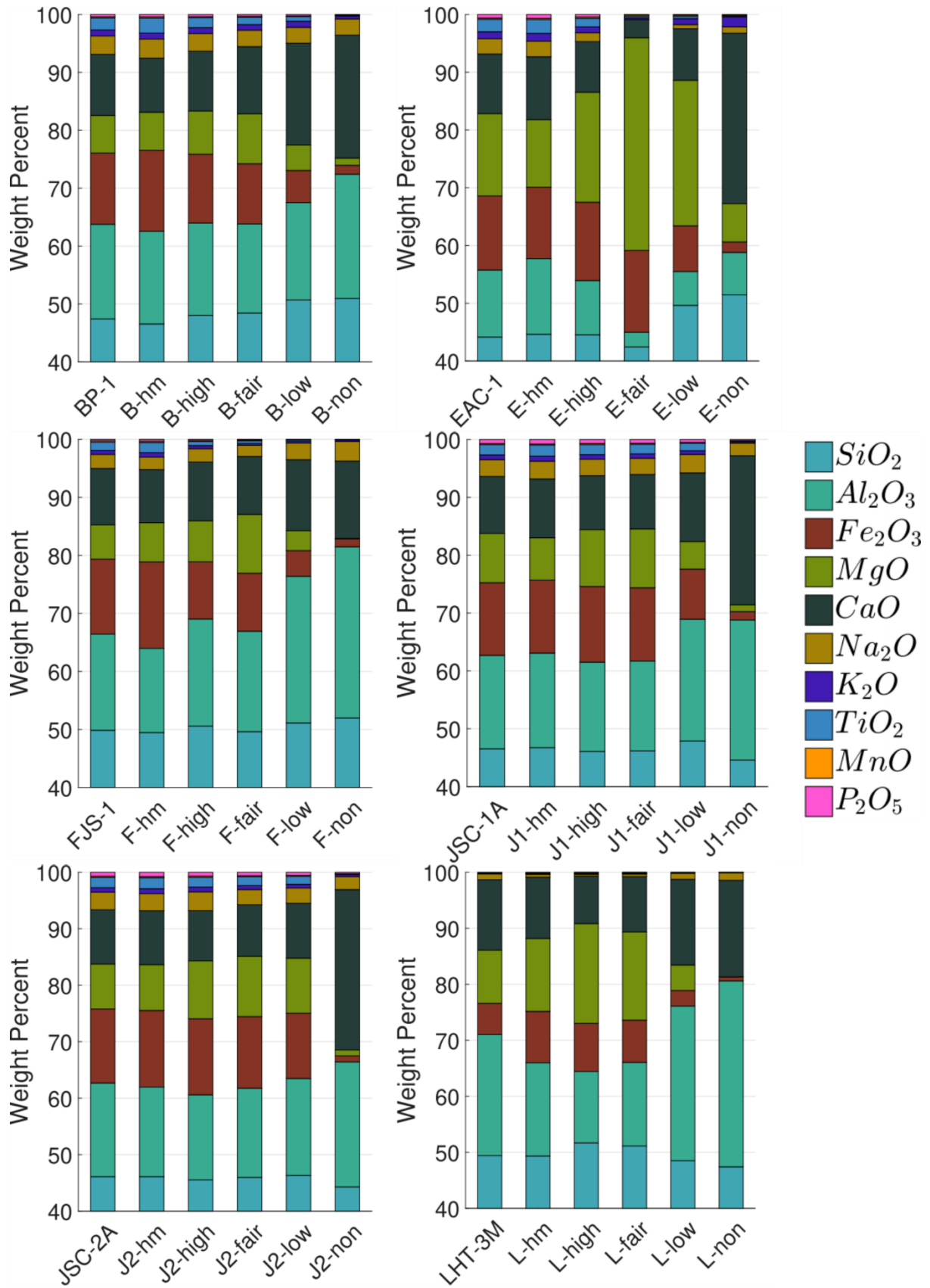
514 To gain a better overview of the effect the magnetic beneficiation had on the regolith simulants,
515 values from Table 4 were taken and translated in the form of stacked bar charts depicted in Figure 10.
516 The values depicted have been corrected for the LOI and rescaled to 100%. Since the SiO₂ content of
517 all samples was always higher than 40%, the first 40% of the samples' compositions are not depicted.
518 Looking at both, Figure 10 and Table 4, differences in magnetic separation of different simulants can
519 be seen. Precise percentage values are listed in Table 4 and the following will discuss rounded values
520 from Figure 10 with the aim of identifying trends focusing on samples that experiences the most
521 drastic changes.

522 Although it was not possible to conduct a detailed mineralogical analysis of the altered samples, due
523 to insufficient amounts of samples, the XRF results presented in Table 4 and in Figure 10 provide
524 insight into which minerals may have been removed in the process. Seen from XRD results in Table 2,
525 in general, all mare simulants utilised consist of mostly pyroxene minerals (both ortho- and clino-),
526 plagioclase feldspar and olivine. Thus, for example, a reduction in iron (titanium) content likely
527 coincides with the removal of the more iron (and possibly titanium) bearing minerals like pyroxenes
528 and/or olivine, in addition to minor/accessory minerals such as spinels (e.g. titanomagnetite and
529 magnetite) and hematite.

530 In general, after magnetic beneficiation the iron oxide content of the simulants at the "non" level (the
531 least magnetic samples) could be reduced to less than 2 wt%, with LHT-3M reaching a value as low as
532 0.72 wt%. Thus, it can generally be assumed that magnetic beneficiation was working. Whether this
533 can be true for actual lunar regolith will be discussed after detailed discussion of the effects of

534 magnetic beneficiation onto the six selected simulant samples. As a reminder, measurements
535 displayed in Table 4 and in Figure 10 were always taken from the tailings, the iron enriched samples
536 of each step and only in the end (“non” samples) taken from the concentrate.

537 Looking at each regolith simulant and the changes over the course of magnetic beneficiation, taking
538 into account XRD results in Table 2 and XRF results from Table 4, changes of each individual simulant
539 are described next:



540

541 Figure 10 Oxides contained in samples (from top left to bottom right BP-1, EAC-1, FJS-1, JSC-1A, JSC-2A and LHT-3M.
 542 Comparison of different stages of magnetic separation: first bar in each chart (unaltered regolith), "-hm", "-high", "-fair", "
 543 -low", "-non"; after unaltered regolith, in decreasing order of magnetic susceptibility. Values below 40 wt% are all SiO_2
 544 content.

545 **BP-1:** From the hand magnet (hm) sample to the “non” sample, iron content gradually decreases from
546 about 14 % to less than 2 %, a relative reduction of more than 80 % compared to the raw regolith with
547 about 12%. Furthermore, MgO and TiO₂ reduced to almost 1 % from >6 % (MgO) and >2% (TiO₂), and
548 in a similar fashion the iron oxide content from 2.1 % to 0.2 %. On the contrary Al₂O₃ and CaO relative
549 fractions increased in “B-non” to 19 % (from about 16 %) for Al₂O₃ and to 19 % (from about 10 %) for
550 CaO. These changes may indicate that B-non mostly consists of anorthite-rich plagioclase feldspar.
551 Coupling of changes in Fe₂O₃ and TiO₂ likely indicate that both are enriched in certain phases. This
552 could be in pyroxene or in smaller amounts of accessory Fe-Ti oxides.

553 **EAC-1:** Similar BP-1, the E-non sample iron oxide content was reduced to almost 2 % compared to the
554 raw regolith of approx. 12%. The two groups showing the most drastic changes are E-fair and E-non.
555 The sample E-fair showed significant relative reductions (shown in brackets) compared to the
556 unaltered bulk for Al₂O₃ (78%), CaO (70%), Na₂O (99%) and K₂O (77%). This likely corresponds to almost
557 complete absence of any feldspar minerals in this sample. On the other hand, iron oxide content as
558 well as MgO of this sample is the highest for all EAC-1 samples analysed, which suggests a large
559 amount of olivine and smaller amounts of pyroxene to be present. For the E-non sample the TiO₂
560 content was 0.13 % (94%). This in combination with changes in other elements suggest low olivine
561 content, high feldspar content and medium pyroxene content.

562 **FJS-1:** For FJS-1, the magnetic separation also worked and gradually lead to a reduction of iron oxide
563 content to less than 2 % in sample F-non, compared to almost 13 % in raw FJS-1. This suggests low to
564 no Fe-bearing pyroxenes and olivine to be present after processing. Further the 29 % of Al₂O₃ suggest
565 that F-non is mostly comprised of feldspar minerals.

566 **JSC-1A & JSC-2A:** Due to JSC-2A intentionally mimicking JSC-1A the composition of these two simulants
567 is similar and are discussed in parallel. The behaviour of those two simulants with respect to magnetic
568 treatment further is also very similar. Similar to the regoliths already described, the Fe-containing
569 phases drop from an initial proportion of approx. 13% to almost 2% in J1-non and J2-non. For both
570 simulants the overall oxide content of the sample did not change drastically from J1/J2-hm to J1/J2-
571 fair and for JSC-2A even until J2-low. Only significant changes to be noticed were in J1-low and J1/J2-
572 non. Compared to the unaltered regolith, for the “-non” samples SiO₂ (~-15/-18%), Fe₂O₃ (~-90/-93%),
573 MgO (~-88/-89%), Na₂O (~-33/-37%), K₂O (~-80/-64%) and TiO₂ (~-90/-93%) decreased relatively (J1/J2)
574 and Al₂O₃ (~+32/+14%) and CaO (~+131/+152%) increased. This suggest that J1/J2-non may be very
575 plagioclase (anorthite) rich since MgO and Fe₂O₃ are at almost zero percent for these samples.

576 **LHT-3M:** The only highland sample, based on plutonic rather than igneous rock started with a lower
577 proportion of iron oxides than the other regoliths. However, this was reduced to less than 1% in

578 sample L-non. Other differences include an increased amount of iron and magnesium oxide in the L-
579 high sample, while at the same time reduced calcium and aluminium oxide content. This suggests an
580 elevated pyroxene content. Further, for L-non almost no Fe₂O₃ or TiO₂, and no MgO was detected at
581 all (n.d.). This suggests that L-non is comprised of almost exclusively plagioclase feldspars with a high
582 amount of anorthosite.

583 From all observations, it seems apparent that it was possible to remove iron-bearing minerals, as
584 targeted for glass production. However, since the change of all simulants' oxide compositions' is
585 different from simulant to simulant, the way magnetically processing might alter regolith on the Moon
586 is expected to be dependent on material composition. For future experiments it will be crucial to
587 measure and observe mineralogy of a simulant in addition to the oxide content as done for this
588 experiment. Since elements are typically contained in certain minerals, magnetic separation separates
589 minerals from each other rather than individual oxides. If the mineral composition of a regolith is
590 known, it should be possible to target and mostly remove certain minerals. Importantly, processing
591 indicates that for many simulants there are coupled changes in Fe₂O₃ and TiO₂. This might indicate
592 that a proportion of the iron in most simulants is present in mixed Fe-Ti-rich phases, facilitating
593 beneficiation. However, although it is possible in theory to preferentially remove certain phases,
594 practically this is complicated by that fact that regoliths are typically composed of igneous rock
595 fragments. Hence, individual regolith grains are most often composed of a multitude of different
596 minerals "glued together", which makes it unlikely that they can be fully separated in practice.
597 Furthermore, the presence of inclusions of Fe-rich oxides in some phases, or the preferential
598 association of oxides with certain phases, can result in variations in the extent to which different
599 phases, and overall composition, is modified during magnetic separation. As such, not just the mineral
600 proportions, but also texture and mineral associations are also important to determine, along with
601 the particulate size distribution. Adaption of any magnetic beneficiating process on the lunar surface
602 would require, therefore, a much fuller understanding of the composition, size distributions, phase
603 relations and textural relationships within lunar regolith.

604 Although, it was not within the scope of this project to increase or concentrate iron oxide content, the
605 method of magnetic separation can also be used to enrich a samples iron oxide content. An additional
606 single test conducted on LHT-3M, aiming at increasing the amount of iron oxide by repeatedly using a
607 hand magnet on it, delivered a sample with an iron oxide content of almost 60 % (59.03 %) after
608 correcting for the LOI. LHT-3M was likely a good simulant for both, iron oxide reduction and increase,
609 due to most of the iron oxide being contained in individual minerals, rather than in igneous rocks. This
610 made the iron bearing minerals accessible to the magnet and led to a good removal rate.

611 How this process may be applicable to actual regolith remains to be tested. Actual lunar regolith will
612 contain iron oxide as well but it may be part of different minerals and/or present as nano phase iron
613 coatings on the regolith's grains surfaces. Furthermore, environmental conditions, especially low
614 temperatures, may be challenging when relying on magnetic susceptibility. Although it cannot be
615 excluded after this study, it seems likely that (other) iron bearing minerals are also magnetically
616 attracted on the lunar surface. Due to the low gravity environment (1/6th of Earth's gravity)
617 susceptibility on the surface may even be better. However, only testing with actual regolith will
618 provide more reliable results whether or not magnetic separation works on actual lunar regolith
619 minerals. Further, with respect to the nano phase iron coating of the grains, magnetic beneficiation
620 as conducted for this study does not seem to be an efficient technique. Instead, attrition grinding may
621 be used to remove these fine dusts and thereby decreasing the overall amount of iron contained in
622 the samples even further. However, this will first need to be tested on suitable regolith simulants and
623 then on actual lunar regolith to provide more reliable data. Last but not least, environmental testing
624 of the described magnetic beneficiation process will need to be conducted to better understand the
625 impact of low temperature low gravitation environment on the process.

626 [Analysis of Optical Properties of Regoliths Simulant Glass](#)

627 **Mechanical properties**

628 After mineral separation and determining changes in oxide/mineral content, LHT-3M samples with
629 the lowest iron oxide contents were used to manufacture glass. As described in the methods sections,
630 flat, parallel, glass sheets were manufactured to, ultimately, assess transparency. Prior to optical
631 measurements of the samples, sample mechanical properties were measured to determine the effect
632 of sample thickness and surface roughness on transparency. To achieve highest transparency, an 'as
633 smooth as possible' surface was desired to avoid light scattering. Although both LHT-3M samples
634 analysed (Figure 8) show higher deviations than the reference microscopy slide, they were both
635 deemed acceptable at a roughness of about 35 nm, compared to about 20 nm of the microscopy slide.
636 Differences between the sample's parallelism are listed in Table 9 and show that the microscopy slide
637 used showed differences in thicknesses of maximum 0.004 mm between its corners. The LHT-3M-1
638 and LHT-3M-2 sample showed maximum differences of 0.034 and 0.021 mm between their corners.
639 Considering that the LHT-3M samples were about half as long as the microscopy slide this leads to an
640 about one order of magnitude difference between the parallelism of the microscopy slide and the
641 LHT-3M-non glass samples. At this level of parallelism, all transparent glass samples were deemed
642 good enough for optical analysis.

643 **Optical**

644 The microscopy slide (marked "Micro" in Figure 9 and Figure 10) showed the overall highest reflectivity
645 measurements, which seems consistent with the surface roughness measurements, showing that the
646 microscopy slide had the smoothest surface compared to LHT-3M-1/2. Compared to the microscopy
647 slide, the two LHT-3M samples (-1 and -2) show a lower reflectivity by about 2-4 % absolute difference,
648 less in the infrared range and more in the UV range (details Figure 10). Further, the contaminated
649 samples (BP-1, FJS-1 and JSC-2A) show similar reflectivity as the other samples, all in the range from
650 about 4% to 8% reflectivity.

651 Transmission results (shown in figure 9) reveal much larger differences between samples than
652 reflectivity. As expected, the microscopy slide shows the highest transmission of all samples. Although,
653 the LHT-3M-3 sample is within only a few percent less reflectivity and next, offset by about 20 %
654 (absolute), the LHT-3M-1/2 samples achieve transmissions of between 60-80 % for most of the
655 measured spectrum. Important to notice, since not clearly visible in Figure 9, the lines of samples LHT-
656 3M-1 and LHT-3M-2 coincide. This is expected due to their very similar geometry/thickness and same
657 geochemical composition. The contaminated samples showed, despite their carbon cloudiness,
658 transmissions between 0 and 15 %. In comparison, other non-beneficiated samples have shown 0%
659 transmission over the entire wavelength range in tests conducted outside this work.

660 Considering the spectral irradiance in space, in the form of the AM0 spectrum depicted in orange in
661 Figure 9, the glasses manufactured from lunar regolith simulant allow most of the energy from the
662 sun to pass the glass in the area of high spectral irradiance. Around 450 nm, the LHT-3M samples show
663 transmission of about 80 % (LHT-3M-3) or 60 % (LHT-3M-1/2). Based on these results, it is fair to say
664 that these glasses are optically transparent and with further improvements to the beneficiation
665 process it may even be possible to achieve similar transparency to terrestrial window or cover glass.

666 Listed in Table 8 in the supplementary material are average transmission versus average thicknesses
667 of the samples. The three samples made of beneficiated LHT-3M show average transmissions of above
668 60 % with the most transparent sample, LHT-3M-3, achieving results of >80 % average transmission.
669 This brings the LHT-3M-3 sample within a range of only 9 % of the reference microscopy slide. Since
670 the LHT-3M-3 sample is only almost half as thick (Table 8 and Table 9) as the LHT-3M-1/2 samples, it
671 seems logical, that it would also allow for the transmission of more light. The increased transmission
672 for thinner samples is thus likely connected to less iron blocking light during transit through the glass.

673 Considering that all LHT-3M samples' transmissions start dropping at about 550 nm compared to the
674 microscopy slide, the average transmission from 550 to 1250 nm is even closer to the microscopy slide
675 in that range than on average. The drop of the samples in this range may be explained by their vestigial
676 iron content, which results in blocking of shorter wavelength light. This suggests that if the iron

677 content can be manipulated accordingly, glass made from regolith is not only transparent but may be
678 engineered to act as a filter over a certain wavelength range. This could be beneficial for applications
679 which require little to no light in the wavelength range <550 nm.

680 From these discoveries, it seems viable to engineer glass from lunar regolith with just the right amount
681 of iron, to be utilised, for example, as cover glass for a solar cell on the lunar surface. Other potential
682 applications include optical filters, windows, building materials, (optical) glass fibres, backplates for
683 mirrors or solar cells and more.

684 Conclusion

685 The results presented in this work successfully show that it is feasible to use lunar in-situ resources to
686 manufacture transparent glass, and open up new possibilities for supporting planetary surface
687 missions to the Moon. Manufactured transparent glass from lunar regolith could be the first raw
688 material which can viably be manufactured on the lunar surface. Having a supply of a raw material as
689 versatile as glass will significantly boost the goal of permanently becoming a multiplanetary species.

690 Optical analysis of transparent glasses manufactured from lunar regolith simulant show, that they are
691 suitable as cover glass for solar cells or general-purpose windows, for example. With these first
692 samples, average transmissions of 80 % were achieved, which was close to the 89% of the reference
693 glass sample. With further optimisation to the beneficiation and manufacturing processes it seems
694 possible to even increase the amount of transmitted light further.

695 Next steps on the way to increasing the technology readiness level (TRL) of transparent glass
696 manufacturing on the lunar surface should include, increasing the amount of regolith processed,
697 improving/tailoring magnetic beneficiation and utilising actual lunar regolith for testing. Further,
698 automating processes as well as environmental testing, such as thermal vacuum tests, will be required.
699 The latter is especially important to test the magnetic susceptibility of minerals at low temperatures,
700 as well as the effect of more reducing atmospheric conditions on glass transparency. Additionally, low
701 gravity testing in the form of a parabola flight or an experiment on the international space station will
702 help to understand process parameters in a low g-environment. Improvements to the magnetic
703 beneficiation process should also, ultimately, make it possible to target specific minerals only and/or
704 reduce elements such as iron or other glass colouration elements further. This would enable further
705 engineering of glass' colour/optical properties, and may allow for glass to be tailored to specific
706 applications.

707 Acknowledgements

708 The authors would like to thank Mike Hall at Edinburgh University for the support with grinding and
709 polishing, as well as Dr. Linda Kirstein at Edinburgh University for providing access to facilities. Further,
710 we like to thank Rob Mueller at NASA Swamp works, for providing the samples of BP-1 and JSC-1A,
711 and Dr. Aidan Cowley and the European Astronaut Centre for providing a sample of EAC-1.

712 Funding

713 This research was co-funded under the ESA NPI scheme together with Heriot-Watt University as well
714 as the Luxembourg National Research Fund and Maana Electric SA.

715 Compliance with ethical standards

716 Conflict of interest: Juergen Schleppi is an employee at Maana Electric. The other authors declare
717 that they have no conflict of interest.

References

- [1] P. D. Kinsman, C. R. Joyner, T. S. Kokan, D. J. Levack and D. E. Morris, "Lunar Surface Logistical Capability: A Study of Spacecraft Needed to Support Human Habitation, Scientific Research, and Commercial Operations on the Lunar Surface," in *AIAA Propulsion and Energy 2019 Forum*, 2019.
- [2] V. Saturn, "Flight manual SA507," *Revised Baseline Manual MSFC-MAN-507*, 1968.
- [3] SpaceX, "SpaceX Homepage," 2020. [Online]. Available: https://www.spacex.com/media/starship_users_guide_v1.pdf. [Accessed 14 December 2020].
- [4] M. Garcia, "International Space Station Facts and Figures," 16 July 2020. [Online]. Available: <https://www.nasa.gov/feature/facts-and-figures>.
- [5] M. Hemsell, "A Concept Study into a Post ISS Architecture," *JBIS*, vol. 69, p. 163–174, 2016.
- [6] A. Zuniga, M. Turner and D. Rasky, "Building an Economical and Sustainable Lunar Infrastructure to Enable Lunar Science and Space Commerce," *Annual Meeting of the Lunar Exploration Analysis Group, held 10-12 October, 2017 in Columbia, Maryland.*, Vols. LPI Contribution No. 2041, id.5006, 2017.
- [7] H. Jones, "The recent large reduction in space launch cost," in *48th International Conference on Environmental Systems*, Albuquerque, New Mexico, 2018.
- [8] B. Hufenbach, T. Reiter and E. Sourgens, "ESA strategic planning for space exploration," *Space Policy*, vol. 30, p. 174–177, 2014.
- [9] M. Shafto, M. Conroy, R. Doyle, E. Glaessgen, C. Kemp, J. LeMoigne and L. Wang, "Draft modeling, simulation, information technology & processing roadmap," *Technology Area*, vol. 11, 2010.
- [10] R. S. Jakhu, J. N. Pelton and Y. O. M. Nyampong, *Space mining and its regulation*, Springer, 2017.
- [11] K. Zacny, "Lunar drilling, excavation and mining in support of science, exploration, construction, and in situ resource utilization (ISRU)," in *Moon*, Springer, 2012, p. 235–265.
- [12] I. A. Crawford, "Lunar resources A review," *Progress in Physical Geography*, vol. 39, pp. 137–167, 2015.
- [13] G. B. Sanders, K. A. Romig, W. E. Larson, R. Johnson, D. Rapp, K. R. Johnson, K. Sacksteder, D. Linne, P. Curreri, M. Duke and others, "Results from the NASA capability roadmap team for in-situ resource utilization (ISRU)," in *International Lunar Conference*, League City, Texas, 2005.
- [14] W. Phinney and D. Criswell, "Lunar resources and their utilization," in *3rd Conference on Space Manufacturing Facilities*, Princeton, NJ, U.S.A., 1977.
- [15] M. Anand, I. A. Crawford, M. Balat-Pichelin, S. Abanades, W. van Westrenen, G. Péraudeau, R. Jaumann and W. Seboldt, "A brief review of chemical and mineralogical resources on the Moon

and likely initial In Situ Resource Utilization (ISRU) applications," *Planetary and Space Science*, vol. 74, p. 42–48, 2012.

- [16] L. Schlüter and A. Cowley, "Review of techniques for In-Situ oxygen extraction on the moon," *Planetary and Space Science*, vol. 181, p. 104753, 2020.
- [17] H. Läkka, "Fibrous Habitat Structure from Lunar Basalt Fibre Hanna Läkka*, Jürgen Schleppeib, Aidan Cowleyc, Lauren Vasey, Maria Yabloninad, Achim Mengesd," *69th International Astronautical Congress (IAC), Bremen, Germany*, no. IAC-18-E5.1.8 x48245, 2018.
- [18] D. Tucker, E. Ethridge and H. Toutanji, "Production of glass fibers for reinforcement of lunar concrete," in *44th AIAA aerospace sciences meeting and exhibit*, 2006.
- [19] L. A. Haskin, "Lunar resources glass and ceramics - NASA Ames Research Center," 1992. [Online]. Available: <https://space.nss.org/settlement/nasa/spaceresvol3/glassnrcer1.htm>. [Accessed 14 December 2020].
- [20] J. Schleppe, J. Gibbons, A. Groetsch, J. Buckman, A. Cowley and N. Bennett, "Manufacture of glass and mirrors from lunar regolith simulant," *Journal of Materials Science*, vol. 54, p. 3726–3747, 2019.
- [21] L. Caprio, A. G. Demir, B. Previtali and B. M. Colosimo, "Determining the feasible conditions for processing lunar regolith simulant via laser powder bed fusion," *Additive Manufacturing*, vol. 32, p. 101029, 2020.
- [22] M. Fateri and A. Gebhardt, "Process Parameters Development of Selective Laser Melting of Lunar Regolith for On-Site Manufacturing Applications," *International Journal of Applied Ceramic Technology*, vol. 12, p. 46–52, 2015.
- [23] J. Mackenzie and R. Claridge, "Glass and ceramics from lunar materials," in *4th Conference on Space Manufacturing Facilities Princeton University*, Princeton, NJ, U.S.A., 1979.
- [24] E. Le Bourhis, *Glass: mechanics and technology*, John Wiley & Sons, 2014.
- [25] G. Heiken, D. Vaniman and B. M. French, *Lunar sourcebook: A user's guide to the Moon*, CUP Archive, 1991.
- [26] J. W. Delano, "Pristine lunar glasses: Criteria, data, and implications," *Journal of Geophysical Research: Solid Earth*, vol. 91, p. 201–213, 1986.
- [27] D. Stöffler, "Glasses formed by hypervelocity impact," *Journal of Non-Crystalline Solids*, vol. 67, p. 465–502, 1984.
- [28] A. E. Saal, E. H. Hauri, M. L. Cascio, J. A. Van Orman, M. C. Rutherford and R. F. Cooper, "Volatile content of lunar volcanic glasses and the presence of water in the Moon's interior," *Nature*, vol. 454, p. 192–195, 2008.
- [29] E. H. Hauri, A. E. Saal, M. J. Rutherford and J. A. Van Orman, "Water in the Moon's interior: Truth and consequences," *Earth and Planetary Science Letters*, vol. 409, p. 252–264, 2015.

- [30] A. D. Saunders and J. Tarney, "Geochemical characteristics of basaltic volcanism within back-arc basins," *Geological Society, London, Special Publications*, vol. 16, p. 59–76, 1984.
- [31] F. A. Frey, N. Walker, D. Stakes, S. R. Hart and R. Nielsen, "Geochemical characteristics of basaltic glasses from the major and famous axial valleys, Mid-Atlantic Ridge (36°–37° N): Petrogenetic implications," *Earth and Planetary Science Letters*, vol. 115, p. 117–136, 1993.
- [32] S.-S. Sun, R. W. Nesbitt and A. Y. Sharaskin, "Geochemical characteristics of mid-ocean ridge basalts," *Earth and Planetary Science Letters*, vol. 44, p. 119–138, 1979.
- [33] D. J. M. Burkhard, "Crystallization and oxidation of Kilauea basalt glass: processes during reheating experiments," *Journal of Petrology*, vol. 42, p. 507–527, 2001.
- [34] S. Yilmaz, O. T. Özkan and V. Günay, "Crystallization kinetics of basalt glass," *Ceramics International*, vol. 22, p. 477–481, 1996.
- [35] J. E. Ericson, A. Makishima, J. D. Mackenzie and R. Berger, "Chemical and physical properties of obsidian: a naturally occurring glass," *Journal of Non-Crystalline Solids*, vol. 17, p. 129–142, 1975.
- [36] A. K. Bandyopadhyay, J. Zarzycki, P. Auric and J. Chappert, "Magnetic properties of a basalt glass and glass-ceramics," *Journal of Non-Crystalline Solids*, vol. 40, p. 353–368, 1980.
- [37] S. K. Kirthika and S. K. Singh, "Experimental Investigations on Basalt Fibre-Reinforced Concrete," *Journal of The Institution of Engineers (India): Series A*, vol. 99, p. 661–670, 2018.
- [38] R. O. Lokken, L. A. Chick and L. E. Thomas, "Development and characterization of basalt-glass ceramics for the immobilization of transuranic wastes," Pacific Northwest Laboratory operated by Battelle, Richland, Washington 99352, 1982.
- [39] S. Muthesius, *Victorian Glassworlds: Glass Culture and the Imagination 1830–1880 by Isobel Armstrong: Oxford: Oxford University Press, 2008, pp. 472*, Taylor & Francis, 2010.
- [40] S. C. Rasmussen, "Origins of Glass: Myth and Known History," in *How Glass Changed the World*, Springer, 2012, p. 11–19.
- [41] J. Henderson, "The raw materials of early glass production," *Oxford Journal of Archaeology*, vol. 4, p. 267–291, 1985.
- [42] L. A. B. Pilkington, "Review lecture. the float glass process," *Proceedings of the Royal Society of London. Series A, Mathematical and Physical Sciences*, vol. 314, p. 1–25, 1969.
- [43] Y.-Z. Yue, "Characteristic temperatures of enthalpy relaxation in glass," *Journal of Non-Crystalline Solids*, vol. 354, p. 1112–1118, 2008.
- [44] H. Bach and N. Neuroth, *The Properties of Optical Glass*, Springer Berlin Heidelberg, 2012.
- [45] K. J. Rao, *Structural Chemistry of Glasses*, Elsevier Science, 2002.
- [46] J. K. Yang, X. H. An, Y. L. Liu and H. L. Zhao, "Analysis and Calculation of Melting Performance for the Low-iron Glass," *J. Mater. Sci. Eng*, vol. 4, p. 034, 2009.

- [47] J.-J. M. P. C. A. Pierre Combes, "Colored glass compositions and glazings produced therewith". Patent US5352640A, 4 10 1990.
- [48] E. Suescun-Florez, S. Roslyakov, M. Iskander and M. Baamer, "Geotechnical properties of BP-1 lunar regolith simulant," *Journal of Aerospace Engineering*, vol. 28, p. 04014124, 2014.
- [49] V. S. Engelschiøn, S. R. Eriksson, A. Cowley, M. Fateri, A. Meurisse, U. Kueppers and M. Sperl, "EAC-1A: A novel large-volume lunar regolith simulant," *Scientific reports*, vol. 10, p. 1–9, 2020.
- [50] V. E. Nash, A. Cowley, M. Fateri, S. Coene, S. Siarov and S. Cristoforetti, "Human Exploration Initiatives at EAC: Spaceship EAC and the Development of Large-Volume Lunar Regolith Simulant for LUNA," *EPSC*, p. EPSC2017–463, 2017.
- [51] H. Kanamori, S. Udagawa, T. Yoshida, S. Matsumoto and K. Takagi, "Properties of lunar soil simulant manufactured in Japan," in *Space 98*, 1998, p. 462–468.
- [52] X. Zeng, C. He, H. Oravec, A. Wilkinson, J. Agui and V. Asnani, "Geotechnical properties of JSC-1A lunar soil simulant," *Journal of Aerospace Engineering*, vol. 23, p. 111–116, 2009.
- [53] S. M. Genco, *Lunar Simulants and Custom Synthetics*, 2016.
- [54] X. Zeng, C. He and A. Wilkinson, "Geotechnical properties of NT-LHT-2M lunar highland simulant," *Journal of Aerospace Engineering*, vol. 23, p. 213–218, 2010.
- [55] K. Norrish and J. T. Hutton, "An accurate X-ray spectrographic method for the analysis of a wide range of geological samples," *Geochimica et cosmochimica acta*, vol. 33, p. 431–453, 1969.
- [56] D. B. Stoesser, D. L. Rickman and S. Wilson, "Preliminary geological findings on the BP-1 simulant," NASA USGS, MSFC Huntsville, Alabama, 2010.
- [57] J.-P. Williams, D. A. Paige, B. T. Greenhagen and E. Sefton-Nash, "The global surface temperatures of the moon as measured by the diviner lunar radiometer experiment," *Icarus*, vol. 283, p. 300–325, 2017.
- [58] A. R. Vasavada, J. L. Bandfield, B. T. Greenhagen, P. O. Hayne, M. A. Siegler, J.-P. Williams and D. A. Paige, "Lunar equatorial surface temperatures and regolith properties from the Diviner Lunar Radiometer Experiment," *Journal of Geophysical Research: Planets*, vol. 117, pp. 1-12 E00H18, 2012.
- [59] Z. Ran and Z. Wang, "Simulations of lunar equatorial regolith temperature profile based on measurements of Diviner on Lunar Reconnaissance Orbiter," *Science China Earth Sciences*, vol. 57, p. 2232–2241, 2014.
- [60] G. Kletetschka and P. J. Wasilewski, "Grain size limit for SD hematite," *Physics of the Earth and Planetary Interiors*, vol. 129, p. 173–179, 2002.
- [61] F. J. Morin, "Magnetic susceptibility of α Fe₂O₃ and α Fe₂O₃ with added titanium," *Physical Review*, vol. 78, p. 819, 1950.

- [62] M. Fateri, S. Pitikaris and M. Sperl, "Investigation on wetting and melting behavior of lunar regolith simulant for additive manufacturing application," *Microgravity Science and Technology*, vol. 31, p. 161–167, 2019.
- [63] C. Ma and G. R. Rossman, "Grossmanite, $\text{CaTi}_3\text{AlSiO}_6$, a new pyroxene from the Allende meteorite," *American Mineralogist*, vol. 94, p. 1491–1494, 2009.
- [64] G. D. Bromiley and A. A. Shiryaev, "Neutron irradiation and post-irradiation annealing of rutile (TiO_2-x): effect on hydrogen incorporation and optical absorption," *Physics and Chemistry of Minerals*, vol. 33, p. 426–434, 2006.

720

721

722

723

Supplementary material

Table 5 Oxide composition of the utilised simulant, manufacturer information in weight % (wt%). All iron contained is collectively listed under Fe₂O₃. No further information on Loss of Ignition (LOI) or more detailed information were provided.

Simulant	SiO ₂	Al ₂ O ₃	Fe ₂ O ₃	MgO	CaO	Na ₂ O	K ₂ O	TiO ₂	MnO	P ₂ O ₅
BP-1	43.0-	16.4-	9-	5.6-	9.2-					
	47.2	18.0	11.7	10.0	14.0	3.45	0-1.1	-	-	-
EAC-1	43.7	12.6	12.0	11.9	10.8	2.9	1.3	2.4	0.2	0.6
FJS-1	49.1	16.2	13.1	3.8	9.1	2.8	1.0	1.9	0.2	0.4
JSC-1A		14.5-	10-	8.5-			0.75-		0.15-	0.6-
	46-49	15.5	11.5	9.5	10-11	2.5-3	0.85	1-2	0.20	0.7
JSC-2A		14.5-	10-	8.5-			0.75-		0.15-	0.6-
	46-49	15.5	11.5	9.5	10-11	2.5-3	0.85	1-2	0.20	0.7
LHT-3M	46.7	24.4	4.2	7.9	13.6	1.3	0.1	0.4	0.1	0.2

Table 6 Yields for magnetic sample separation, shown in grams. Out of initially 200 grams unaltered regolith simulant only the grainsize fraction of 500 to 63 µm was processed and the amounts left after sieving are listed under "start". Each simulant type was split into 5 groups, "HM" (hand magnet), "high", "fair", "low" and "non" with descending order of magnetic susceptibility. The measured samples were taken from the tailings (the material with higher magnetic susceptibility after each run. Under "loss" the amount of material lost during processing is listed.

500-63	start	HM	high	fair	low	non	loss
BP-1	123.4	62.0	42.0	7.6	2.7	3.1	6.0
EAC-1	132.8	96.9	22.9	9.7	1.3	0.4	1.6
FJS-1	96.2	69.0	6.2	3.9	8.5	5.6	3.0
JSC-1A	114.3	25.1	49.8	33.9	2.6	0.5	2.4
JSC-2A	113.6	24.9	63.7	22.9	0.3	0.3	1.5
LHT3M	129.7	2.7	17.1	50.3	14.2	44.4	1.0

Table 7 Loss on ignition of samples magnetically altered, in wt%

Sample	BP-1	B-hm	B-high	B-fair	B-low	B-non
LOI	2.04	0.88	2.22	3.76	9.11	9.80
Sample	EAC-1	E-hm	E-high	E-fair	E-low	E-non
LOI	1.40	1.19	1.74	1.08	6.05	20.31
Sample	FJS-1	F-hm	F-high	F-fair	F-low	F-non
LOI	-0.25	-0.19	-0.16	-0.37	-0.04	0.22

Sample	JSC1A	J1-hm	J1-high	J1-fair	J1-low	J1-non
LOI	-0.46	-0.46	-0.57	-0.67	-0.20	11.11
Sample	JSC-2A	J2-hm	J2-high	J2-fair	J2-low	J2-non
LOI	-0.79	-0.65	-0.64	-0.70	-0.46	14.05
Sample	LHT-3M	L-hm	L-high	L-fair	L-low	L-non
LOI	0.12	-0.36	2.22	0.21	0.26	0.25

Table 8 Average transmission and thickness of transparent glasses. Thickness is shown in mm.

Sample	BP-1	FJS-1	JSC-2A	LHT-3M-1	LHT-3M-2	LHT-3M-3	Micro
Avg. trans.	10.72%	4.07%	7.17%	60.86%	60.57%	80.58%	89.01%
Avg. thick.	1.336	1.321	1.341	1.400	1.385	0.838	1.075

Table 9 Dimensions of transparent glasses all samples 3*LHT-3M, BP-1, FJS-1, JSC-1 and microscopy slide ("Micro") are listed in mm. Show are length, width, thickness at all four corners and average thickness (t_{avg}) of the samples.

Sample	Length	Width	t_{LF}	t_{LB}	t_{RF}	t_{RB}	t_{avg}
BP-1	24.2	18.1	1.353	1.346	1.323	1.320	1.336
FJS-1	33.7	21.1	1.314	1.343	1.303	1.322	1.321
JSC-2A	26.7	15.0	1.345	1.353	1.336	1.330	1.341
LHT-3M-1	34.5	19.0	1.391	1.391	1.412	1.404	1.400
LHT-3M-2	29.8	19.8	1.396	1.370	1.403	1.369	1.385
LHT-3M-3	18.9	19.6	0.833	0.838	0.839	0.843	0.838
Micro	75.8	21.9	1.077	1.073	1.074	1.075	1.075

L: left, R: right, B: back, F: front, avg: average